1986A&AS....64..135P

ASTRONOMY & ASTROPHYSICS
SUPPLEMENT SERIES

Astron. Astrophys. Suppl. Ser. **64**, 135-171 (1986)

VLA observations of low luminosity radio galaxies.
I. Sources with angular size smaller than two arcminutes

P. Parma ([1]), H. R. de Ruiter ([1]), C. Fanti ([1,2]) and R. Fanti ([1,2])

([1]) Istituto di Radioastronomia, Via Irnerio, 46, 40126 Bologna, Italy
([2]) Dipartimento di Astronomia, Universita' di Bologna, Via Zamboni 33, 40126 Bologna, Italy

Received June 17, accepted August 27, 1985

Summary. — Fifty seven radio sources with angular size smaller than about two arcmin, selected from two complete samples of low luminosity B2 radio galaxies, have been observed at 20 cm with the VLA in the B configuration, with an angular resolution of about 3.5 arcsec. We describe here the reduction procedure and discuss the quality of the radio maps. The dynamic range in the final CLEANed maps is usually around 100 : 1 or better. Observational parameters and intrinsic properties derived for each source are given in separate tables. Contour maps are presented for resolved sources. Information on individual sources is provided, particularly in case of interesting structures.

Key words : radio galaxies.

1. Introduction.

Much work on low luminosity radio galaxies has been based on two samples of radio sources from the B2 Catalogue (Colla *et al.*, 1970, 1972, 1973). The first sample, also called the « bright » sample, was presented in papers by Fanti *et al.* (1973) and Colla *et al.* (1975a, 1975b). It consists of elliptical galaxies from the Zwicky catalogue (Zwicky *et al.*, 1963, 1966, 1968) brighter than about 15.7 (m_{pg}). The second sample, which includes sources optically identified with fainter galaxies down to about 16.5 mag in the visual, was discussed in Fanti *et al.* (1978). Both samples contain radio sources that were originally selected at 408 MHz as having a flux density greater than 0.2 Jy. Since the sky areas of the two samples partially overlap, galaxies with $m_{pg} < 15.7$ might belong to both samples. Being already part of the bright sample, these were not repeated in the list of galaxies of the faint sample, which therefore mainly contains elliptical galaxies with magnitudes between $m_{pg} = 15.7$ and $m_v = 16.5$. The associated radio sources are therefore, on average, slightly more distant and luminous than those in the bright sample.

We refer to the original articles for details and give here only a short summary of the relevant information.

Twelve-hour synthesis observations of all radio galaxies from the bright sample with angular size larger than two arcmin were made with the Westerbork Synthesis Radio Telescope (WSRT) and were discussed by Ekers *et al.* (1981). For the remaining sources only WSRT short cut observations existed up till now (Fanti *et al.*, 1977; Fanti *et al.*, 1978; Feretti *et al.*, 1983). Although several individual B2 sources have been studied in great detail at various wavelengths by many authors, no homogeneous study has been done in the radio over the entire collection of low luminosity B2 radio galaxies, using the high sensitivity and angular resolution of the VLA.

For this reason we undertook an observational program intended to produce radio maps with a resolution ranging from ~ 1 arcsec for the most compact sources to ~ 13 arcsec for the most extended ones. The aim is to produce parameters that can be used to determine overall properties of low luminosity radio galaxies, such as frequency of occurrence of radio jets, morphological characteristics like bending, distortions, presence of hot spots, etc. These properties should be studied as a function of other physical quantities, such as luminosity, linear size, etc. The existence of two statistically complete samples makes this goal feasible.

In the present paper we discuss the first instalment : observations of sources (57) with angular size smaller than about two arcmin, from both the bright and faint sample, with a resolution of ~ 3.5 arcsec, at the observing frequency of 1465 MHz. The other observations, partly with higher and partly with lower resolution, will be presented in forthcoming papers.

In section 2 we give details on the observational procedure and data reduction. In section 3 we give the results in the form of radio maps and tables where the observed and intrinsic radio source parameters are summarized. Finally, we give comments on a number of sources in section 4.

Send offprint request to : P. Parma.

2. Observations and data reduction.

Sources from the two aforementioned samples, having angular size smaller than two arcmin, were selected for observation in snap-shot mode with the VLA in the B configuration. Each observation had a duration ranging from ~ 10 to ~ 70 min, depending on known source characteristics.

For a description of the VLA and its modes of operation we refer to Thompson *et al.* (1980).

The observations were carried out in August and September 1982, at the frequency of 1465 MHz, with a bandwidth of 50 MHz. The synthesized beam is about 3-4 arcsec. With this bandwidth and observing frequency time losses due to the averaging period (we used a 30 s integration time) are negligible. Losses of peak intensity due to bandwidth smearing are at most 10 % at a radial distance of 1 arcmin from the phase center. The sources discussed here have an angular diameter less than 2 arcmin, so that in general corrections to the flux densities are small (at most a few per cent). For this reason no correction for bandwidth smearing was applied.

A calibration source was observed immediately before or after the program source. Their separation in the sky was usually less than 10°, in order to minimize the disturbing effects of the atmosphere. The flux densities were brought on the scale of Baars *et al.* (1977). As primary flux calibrators we periodically observed 3C 286 and 3C 138; flux densities of secondary calibrators were bootstrapped from the flux densities of 3C 286 and 3C 138.

Raw data were checked for deviating amplitudes and phases, which were edited out.

For a typical 10-min observation the rms receiver noise is 0.18 mJy/beam.

All post-calibration reduction was done with the Vax 11/780 computer of the Istituto di Radioastronomia del CNR (Bologna), using the NRAO Astronomical Image Processing System (AIPS). A typical reduction sequence consisted of the following steps :

a) the visibility amplitudes of each source were visually checked and, if necessary, deviating points were deleted;

b) the visibilities were Fourier transformed and a « dirty » map of the total intensity was produced. The gridded UV data were first averaged in cells of 3 by 3 pixels, in order to give a higher weight to the longest baselines, thus improving the resolution although at the cost of a slightly higher noise (Sramek, 1982). Usually a map size of 512 by 512 pixels was sufficient, using a step size of one arcsec. However, sometimes a strong confusing source was present, which required maps 1024 × 1024 pixels in size. In a minority of cases strong known confusing sources at larger distance from the field center were removed by subtraction from the UV data;

c) the Fourier transform of the visibilities always needed further processing, since for snap-shot observations the sidelobe level is quite high. The « dirty » map was therefore always CLEANed, following the recipe of Clark (1980). The CLEAN was halted when the sum of the CLEAN components' flux density showed convergence. At this stage the « residual map » was generally consistent with the expected noise;

d) a number of strong sources required, in addition, self-calibration. The resulting dynamic range was then often better than 100 : 1 after one or two self-calibration iterations.

At present we have not carried on a systematic analysis of polarization since the signal to noise ratio is not adequate to study the whole source sample. Nevertheless in several cases a significant polarization was found. These results will be presented elsewhere.

The source list, the observing time per source, the actual rms noise in each map, and the FWHM of the synthesized beam are given in tables Ia and Ib for the bright and the faint sample respectively. When the VLA observations are limited by dynamic range the actual noise in a map is higher than the receiver noise even after a number of self-calibration cycles.

3. Results.

Measured parameters for the sources and, when possible and reliable, also for their sub-components (whose definition is, however, sometimes quite subjective) are given in tables IIa and IIb. The first line gives optical data and radio information on the whole source. The following lines refer to radio sub-components. The meaning of the columns is self-explanatory.

We give the positions of the associated optical galaxy, of the source radio core, and, occasionally, of the hot-spots.

The total flux densities were calculated by integration over the entire source region or, when appropriate, over the map portion comprising a sub-component.

A comparison of the VLA fluxes with those measured with the WSRT at the same frequency, but with lower resolution (24 arcsec), showed good agreement (usually within 10 %) between the two sets of data. However, six sources (0800+24, 1339+26, 1506+34, 1610+29, 1658+32, 2116+26) have VLA total fluxes from $\sim 20\,\%$ to $\sim 50\,\%$ lower than those measured with the WSRT, indicating that extended low brightness features have been missed in the present observations.

Diameters at half maximum (i.e. FWHM) were determined by means of gaussian fits for the cores and, occasionally, for well defined components (e.g. hot-spots in the lobes), that is, for all components that can be approximated well by a gaussian. Sizes smaller than about one arcsec may be very uncertain. We still report them in table II to give an idea of the source compactness. In all other cases we measured for each source or sub-component the angular size defined by the lowest reliable contour (LAS). The angular size thus defined is more ambiguous, due to the nature of low luminosity radio sources : they are often edge-darkened, i.e. they gradually fade out into the background. The angular size may therefore depend on the observation itself (observing time, quality) and its determination necessarily is subjective.

Pictures of the B2 sources, except for those which are unresolved or slightly resolved, are given in figure 1a and 1b in the form of contour maps. The value of the contour levels is always expressed in mJy/beam.

The cross denotes the optical position of the galaxy. Its accuracy depends on the extent of the optical image on the

Palomar Sky Survey Prints and is expected to be not better than a few arcsec.

On the basis of the present observations the identification of two sources (B2 1506+34 and B2 1358+28) should be considered as uncertain. Two other sources, instead, were found to be clearly not associated with the galaxies originally suggested as identifications. They are : B2 0916+34, from the bright sample, and B2 1225+26 from the faint sample. These two sources are not given in the tables, nor in figure 1.

Intrinsic source parameters, generally rounded to the closest integer or half integer value, are given in tables IIIa and IIIb. Linear sizes were derived from data in table II. Internal energy density and magnetic field were determined for well resolved sub-components with standard formulae, using the assumption of equipartition (Pacholczyk, 1970) and further assuming that :

1) the radio spectrum can be represented by a power law from 10 MHz to 100 GHz;

2) the ratio between proton and electron energy is 1;

3) the radiative volume can be approximated by an ellipsoid with the major axis in the plane of the sky.

Thus, apart from the assumption of equipartition itself, the adopted geometry of the emitting volume and the electron/proton ratio represent additional uncertainties for the determination of intrinsic source parameters, which, as is well known, could change by many orders of magnitude. The precision with which the internal energy density and magnetic field are given in table III derives from the accuracy of the observed parameters (brightness, linear size).

The adopted value for the Hubble constant is $H = 100$ km s^{-1} Mpc^{-1}.

4. Comments on individual sources.

4.1 The bright sample.

0120 + 33. — The radio galaxy (NGC 507) is located in the Zwicky Cluster 0107 + 3212, and is the brightest (or second brightest) galaxy in a very dense region : there are 80 galaxies with magnitude $m_{pg} < 15.7$ within a projected distance of 1.5 Mpc from NGC 507. This is the so called Pisces Group.

The radio emission is very faint and diffuse : the surface brightness is of the order of 0.05 mJy per square arcsec. The radio spectrum of the source is very steep (Ekers *et al.*, 1981). Although the radio structure is clearly very distorted, a more detailed study of the source morphology is difficult, due to its faintness.

0149+35. — Brightest galaxy in the cluster Abell 262; it has a dust lane in position angle $\sim -4°$. (Battistini *et al.*, 1980), roughly perpendicular to the radio axis.

0206+35. — This radio galaxy consists of a core with a two-sided jet, embedded in a large symmetric halo of diffuse emission. The optical galaxy shows evidence of a dust lane (Battistini *et al.*, 1980) which is parallel to the inner optical major axis and roughly perpendicular to the jet.

0207+38. — Although this radio source was included in the complete sample of elliptical galaxies (Colla *et al.*, 1975), the parent galaxy is clearly more similar to an S0 or to a spiral galaxy : it has been called a post-eruptive Sa (Zwicky and Kowal, 1968) or a distorted Sa (de Vaucouleurs *et al.*, 1975). Indeed, the radio structure might be classified as disk-like. There is no sign of either a radio core or of jets or radio lobes. The optical image of the galaxy has a diameter of about one arcmin. The optical center is not well defined on the Sky Survey print and for that reason the difference between the position of the radio and of the optical center is not significant.

0222+36. — The radio source is slightly resolved and has a flat spectrum; no map is given in figure 1.

0258+35. — The radio source is slightly resolved and has a flat spectrum; no map is given in figure 1.

0331+39. — The radio structure is rather peculiar : the source consists of a resolved core plus a faint halo ~ 1 arcmin in diameter. Our more recent high resolution observations (~ 1.5 arcsec) show an identical structure, but at the scale of the present map resolved core. This suggests that the entire source can be represented by a single gaussian component.

0648+27. — The radio source is slightly resolved and its map is not given. Its radio spectrum is straight from 1.4 to 5.0 GHz, but shows self-absorption at lower frequencies.

0722 + 30. — The galaxy is classified as SO. The radio structure resembles that of 0149+35 : both 0722+30 and 0149+35 are strongly distorted close to the nucleus (De Ruiter and Parma, 1984). The optical and radio images do not match completely; the major radio axis changes position angle going from 110° (close to the center) to 90° (external part). The optical major axis has a position angle of 135°.

0800+24. — Head-tail radio source observed also by Stocke and Burns (private communication). It lies in a very poor environment, where only 6 galaxies were found in a one cubic Mpc region (Stocke, private communication; Burns, 1983).

0836+29. — This is one of the few sources in the bright B2 sample that show two hot-spots. The low brightness region to the west of the southern component was also visible in a 5.0 GHz WSRT map (Fanti *et al.*, 1977). A study of the emission lines originating from the radio emitting volumes has been done by van Breugel and Heckman (1982).

1040+31. — The radio morphology is quite peculiar. The source is identified with a system of three elliptical galaxies in a common halo (Zwicky *et al.*, 1963). The cross marks the geometrical center of the common envelope. Individual galaxy positions are not available.

1108+27. — The optical identification is with the eastern galaxy of a pair.

1113+29. — The radio source is associated with the northern galaxy of a double system located close to the center of the cluster Abell 1213.

1122+39. — The parent galaxy has a dust lane (Kotanyi and Ekers, 1979) which is almost perpendicular to the radio jets. WSRT observations at 610, 1415 and 4995 MHz are discussed by Kotanyi (1979).

1144+35. — The jet is very faint with respect to the core, its surface brightness being less than 0.5 % of the peak flux density.

1254+27. — The radio galaxy belongs to the Coma cluster and is located at its periphery. The optical image of the galaxy is very large (~ 1 arcmin) and the optical center is therefore poorly defined.

1317+33. — The radio source coincides with the western galaxy of a pair of two ellipticals in a common halo. The radio structure resembles an elongated disk with a major axis that continuously changes position angle.

1318 + 34. — The radio source is slightly resolved. Although the radio and optical positions differ by ~ 8 arcsec, still the identification is probably correct : in fact the optical structure is quite complex (Arp, 1966). No map is given in figure 1.

1346+26. — The radio galaxy is the brightest member (cD galaxy) of Abell 1795. A map with higher resolution has been published by van Breugel *et al.* (1984). Note the dramatic change in structure revealed by the different resolutions of the present map (~ 3.5 arcsec) and the one by van Breugel *et al.* (1984) (~ 0.5 arcsec). These authors also discuss the large scale line emission originating from the radio volumes.

1506+34. — The radio source is almost unresolved and no map is given in figure 1. The flux reported here is 40 % lower than that measured with the WSRT. The radio and optical positions are discrepant by ~ 30 arcsec, therefore the identification should be considered uncertain.

1525+29. — The radio source is associated with the fainter southern galaxy of a double system in a common halo. It is located at the center of the cluster Abell 2079 (Fanti *et al.*, 1983).

1610+29. — The source is associated with the brightest cD central galaxy of Abell 2162. For optical data, see Fanti *et al.* (1982).

1621 + 38. — The diffuse tail has a direction perpendicular to a smaller scale jet emanating from the nucleus. See also Ekers *et al.* (1978) for a discussion of the environment. A high resolution map is given by O'Dea and Owen (1985).

1626+39. — Brightest member of Abell 2199. The peculiar radio morphology was discussed by Burns *et al.* (1983). See also Jaffe and Perola (1974).

1652+39. — The source, unresolved, is associated with the N galaxy Mk 501 ; the radio spectrum is flat. No map is given in figure 1.

1833+32. — The source is more extended than 2 arcmin and has a rather high total radio power (> 1.0 E 25 W/Hz). Its structure is clearly quite different from all the other sources in this sample, and it is rather typical of a high luminosity radio source.

4.2 The faint sample.

0908+37. — See Machalski *et al.* (1983) for a higher resolution map.

1003+26. — The radio source, slightly resolved, is associated with the brightest galaxy in the cluster Abell 923. The radio spectrum is quite steep ($\alpha = 1.3$). No map is given in figure 1.

1037+30. — The source is unresolved. The radio spectral index is 0.9. No map is given in figure 1.

1113+24. — The source is associated with the central brightest galaxy in the Zwicky cluster 1113.0+2452; it shows a complex halo-like structure. The radio spectrum is very steep ($\alpha = 1.5$).

1204+34. — Hot spots are found in both radio lobes : this object starts to resemble a high luminosity radio source.

1303+31. — The radio source is associated with the brightest galaxy in the cluster Abell 1667 (Coma B). Our more recent high resolution observations confirm its head tail structure.

1339 + 26. — Previous observations (Miley and Harris, 1977) showed a head-tail source, which was identified with the eastern member of the close pair of giant galaxies in the cluster Abell 1775. Simon (1979) confirmed the identification and found, in addition, a region of low brightness emission associated with the other galaxy. With the present map, it is clear that there are two distinct radio sources : a head tail and a wide angle tail associated with each of the two galaxies. A high resolution map is given by O'Dea and Owen (1985).

1347+28. — The source is located in the cluster Abell 1800.

1358+28. — The identification is dubious, as the galaxy position is at about 10 arcsec SE of the centroid of an otherwise classical double radio source.

1430+25. — This is a classical head tail source, apparently with a bright spot at the end of the tail (Parma *et al.*, 1985). Our A-array observations suggest that the northern component might be a background object.

1450+28. — The source is associated with the southernmost of a pair of galaxies in the cluster Abell 1984.

1527+30. — This is a wide angle tail located in the cluster Abell 2083.

1557+26. — The source is slightly resolved. Another unresolved source ~ 30 arcsec to the west is probably a background object. No map is given in figure 1.

1658+32. — The source is located in the cluster Abell 2241. The bifurcation of its tail seen by Bijleveld and Valentijn (1982) is confirmed by our map. A high resolution map is given by O'Dea and Owen (1985).

1736+32. — The source is probably a normal triple, the component to the south west possibly being a background source. Our recent A array observations confirm this suspicion.

1747+30. — The northern double is likely to be a background object, although the northern jet curiously points towards it.

Acknowledgements.

P. P. and H. de R. thank the staff at the VLA for their warm hospitality, and in particular express their gratitude to Drs. R. Ekers, E. Fomalont, R. Perley and J. van Gorkom for their continual willingness to help us with advice on data reduction.

The National Radio Astronomy Observatory is operated by Associated Universities, Inc., under contract with the National Science Foundation.

References

ARP, H. C. : 1966, *Astrophys. J. Suppl.* **14,** 1.
BAARS, J. W. M., GENZEL, R., PAULINY-TOTH, I. I. K., WITZEL, A. : 1977, *Astron. Astrophys. Suppl.* **61,** 99.
BATTISTINI, P., BONOLI, F., SILVESTRO, S., FANTI, R., GIOIA, I. M., GIOVANNINI, G. : 1980, *Astron. Astrophys.* **85,** 101.
BIJLEVELD, W., VALENTIJN, E. A. : 1982, *Astron. Astrophys.* **111,** 50.
VAN BREUGEL, W., HECKMAN, T., MILEY, G. K. : 1984, *Astrophys. J.* **276,** 79.
VAN BREUGEL, W. and HECKMAN, T. : 1982, *IAU Symp.* **97** « Extragalactic Radio Sources », ed. by Heeschen and Wade (Reidel) p. 61.
BURNS, J. O. : 1983, *Astrophysical Jets*, ed. by Ferrari and Pacholczyk (Reidel) p. 67.
BURNS, J. O., SCHWENDEMAN, E., WHITE, R. A. : 1983, *Astrophys. J.* **271,** 575.
CLARK, B. G. : 1980, *Astron. Astrophys.* **89,** 377.
COLLA, G., FANTI, C., FANTI, R., FICARRA, A., FORMIGGINI, L., GANDOLFI, E., GRUEFF, G., LARI, C., PADRIELLI, L., ROFFI, G., TOMASI, P., VIGOTTI, M. : 1970, *Astron. Astrophys. Suppl. Ser.* **1,** 281.
COLLA, G., FANTI, C., FANTI, R., FICARRA, A., FORMIGGINI, L., GANDOLFI, E., LARI, C., MARANO, B., PADRIELLI, L., TOMASI, P. : 1972, *Astron. Astrophys. Suppl. Ser.* **7,** 1.
COLLA, G., FANTI, C., FANTI, R., FICARRA, A., FORMIGGINI, L., GANDOLFI, E., GIOIA, I., LARI, C., MARANO, B., PADRIELLI, L., TOMASI, P. : 1973, *Astron. Astrophys. Suppl. Ser.* **11,** 291.
COLLA, G., FANTI, C., FANTI, R., GIOIA, I., LARI, C., LEQUEUX, J., LUCAS, R., ULRICH, M. H. : 1975a, *Astron. Astrophys. Suppl. Ser.* **20,** 1.
COLLA, G., FANTI, C., FANTI, R., GIOIA, I., LARI, C., LEQUEUX, J., LUCAS, R., ULRICH, M. H. : 1975b, *Astron. Astrophys.* **38,** 209.
DE RUITER, H. R., PARMA, P. : 1984, *Astron. Astrophys.* **141,** 189.
EKERS, R. D., FANTI, R., LARI, C., ULRICH, M. H. : 1978, *Astron. Astrophys.* **69,** 253.
EKERS, R. D., FANTI, R., LARI, C., PARMA, P. : 1981, *Astron. Astrophys.* **101,** 194.
FANTI, R., GIOIA, I., LARI, C., LEQUEUX, J., LUCAS, R. : 1973, *Astron. Astrophys.* **24,** 69.
FANTI, C., FANTI, R., GIOIA, I. M., LARI, C., PARMA, P., ULRICH, M. H. : 1977, *Astron. Astrophys. Suppl. Ser.* **29,** 279.
FANTI, R., GIOIA, I., LARI, C., ULRICH, M. H. : 1978, *Astron. Astrophys. Suppl. Ser.* **34,** 341.
FANTI, C., FANTI, R., FERETTI, L., FICARRA, A., GIOIA, I. M., GIOVANNINI, G., GREGORINI, L., MANTOVANI, F., MARANO, B., PADRIELLI, L., PARMA, P., TOMASI, P., VETTOLANI, P. : 1982, *Astron. Astrophys.* **105,** 200.
FANTI, C., FANTI, R., FERETTI, L., GIOIA, I. M., GIOVANNINI, G., GREGORINI, L., PADRIELLI, L., PARMA, P., TOMASI, P., MARANO, B., ZITELLI, V. : 1983, *Astron. Astrophys. Suppl. Ser.* **51,** 179.
FERETTI, L., GIOVANNINI, L., GREGORINI, L., PARMA, P. : 1983, *Astron. Astrophys.* **126,** 311.
JAFFE, W. J. and PEROLA, G. C. : 1974, *Astron. Astrophys.* **32,** 223.
KOTANYI, C. G., EKERS, R. D. : 1979, *Astron. Astrophys.* **73,** L1.
KOTANYI, C. G. : 1979, *Astron. Astrophys.* **74,** 136.
MACHALSKI, J., CONDON, J. J. : 1983, *Astron. J.* **88,** 143.
MILEY, G. K., HARRIS, D. E. : 1977, *Astron. Astrophys.* **61,** L23.
O'DEA, C. P., OWEN, F. N. : 1985, *Astron. J.* **90,** 927.
PACHOLCZYK, A. G. : 1970, Radio Astrophysics (W. H. Freeman & Co.).
PARMA, P., EKERS, R. D., FANTI, R. : 1985, *Astron. Astrophys. Suppl. Ser.* **59,** 511.
SIMON, A. J. B. : 1979, *Monthly Notices Roy. Astron. Soc.* **188,** 637.
SRAMEK, R. A. : *Synthesis Mapping ;* NRAO Workshop-Socorro, New Mexico, June 21-25 1982 ; ed. A. R. Thompson and L. R. D'Addario.
THOMPSON, A. R., CLARK, B. G., WADE, C. M., NAPIER, P. J. : 1980, *Astrophys. J. Suppl.* **44,** 151.
DE VAUCOULEURS, G., DE VAUCOULEURS, A., CORWIN Jr., H. : 1975, *Second Reference Catalogue of Bright Galaxies* (The University of Texas Press, Austin).
ZWICKY, F. and HERZOG, E., 1963, *Catalogue of Galaxies and Clusters of Galaxies*, Vol. 2 (Calif. Inst. of Tech.).
ZWICKY, F. and HERZOG, E. : 1966, *Catalogue of Galaxies and Clusters of Galaxies*, Vol. 3 (Calif. Inst. of Tech.).
ZWICKY, F. and KOWAL, C. : 1968, *Catalogue of Galaxies and Clusters of Galaxies*, Vol. 4 (Calif. Inst. of Tech.).

TABLE Ia. — *Observational parameters.*

Name	Obs.time min	beam arcsec	PA degrees	noise mJy/beam
0120+33 NGC 507	59	3.48 x 3.38	-35	0.35
0149+35 NGC 703	58	3.64 x 3.24	15	0.10
0206+35 4C35.03	35	3.42 x 3.39	-43	0.38
0207+38 NGC 828	11	3.39 x 3.30	65	0.18
0222+36	24	3.28 x 2.84	3	0.15
0258+35 NGC1167 4C34.09	11	3.21 x 3.16	33	1.03
0331+39 4C39.12	31	3.66 x 3.26	-15	0.27
0648+27	56	3.49 x 3.23	-10	0.17
0722+30	58	3.40 x 3.07	5	0.10
0800+24	60	3.83 x 3.78	50	0.15
0836+29 4C29.30	54	4.30 x 3.70	-76	0.28
1040+31	28	3.90 x 3.36	-1	0.28
1108+27	25	3.59 x 3.15	-87	0.11
1113+29 4C29.41	34	3.75 x 3.47	6	0.25
1122+39 NGC3665	21	3.32 x 2.88	6	0.13
1144+35	9	3.44 x 3.27	64	0.24
1254+27 NGC4839	14	4.01 x 3.27	-81	0.20
1317+33 NGC5098	60	3.30 x 3.22	-34	0.17
1318+34	15	4.24 x 4.22	-46	0.35
1322+36 NGC5141 4C36.24	12	3.97 x 3.73	-23	0.34
1346+26 4C26.42	31	3.30 x 2.99	14	0.19
1506+34	25	3.80 x 3.80	37	0.34
1525+29	33	3.64 x 3.25	-3	0.12
1553+24	69	3.45 x 3.26	-8	0.11
1610+29 NGC6086	35	6.50 x 4.80	-89	0.15
1621+38 NGC6137	34	3.47 x 3.30	-36	0.20
1626+39 NGC6166 3C338	31	4.02 x 3.93	-85	1.00
1652+39 4C39.49	11	3.82 x 3.65	-25	1.05
1833+32 3C382	33	3.36 x 3.31	-40	1.00
1855+37	29	3.87 x 3.36	-11	0.32
2116+26	34	3.59 x 3.52	30	0.20
2236+35	62	2.98 x 2.95	48	0.08

TABLE Ib. — *Observational parameters.*

Name	Obs.time min	beam arcsec	PA degrees	noise mJy/beam
0708+32	63	3.13 x 2.97	26	0.15
0908+37	14	3.46 x 3.31	58	0.13
0913+38	19	3.31 x 2.87	6	0.14
1003+26	56	3.50 x 3.38	30	0.19
1037+30	29	3.69 x 3.32	14	0.45
1113+24	34	3.48 x 3.44	39	0.09
1204+24	43	3.27 x 3.05	25	0.08
1204+34	32	3.3x 2.89	6	0.12
1303+31	63	3.43 x 3.23	11	0.15
1339+26	59	3.61 x 3.30	-3	0.20
1347+28	32	3.48 x 3.42	84	0.12
1358+28	23	4.16 x 4.00	28	0.26
1430+25	34	3.84 x 3.73	-84	0.25
1450+28	57	3.32 x 2.93	5	0.11
1527+30	74	3.39 x 3.33	-40	0.14
1557+26	58	3.53 x 3.41	-30	0.14
1609+31	38	3.72 x 3.71	-50	0.23
1613+27	28	3.77 x 3.74	-51	0.32
1638+32	19	4.26 x 3.94	74	0.19
1658+32	22	4.22 x 4.16	22	0.20
1736+32	30	4.15 x 3.71	-73	0.24
1747+30	58	4.31 x 4.17	-37	0.30
1752+32	33	3.59 x 3.38	-17	0.16

TABLE IIa. — *Observational data.*

NAME	R.A. h m sec	DEC. ° ' "	z	m_{pg}	S(1.4) mJy	Size FWHM arcsec	Size P.A. deg.	LAS arcsec
0120+33	01 20 50.7	32 59 45	0.0164	13.0	60			95
NGC 507								
core	01 20 50.9	32 59 43			2			
E lobe					22			39 x 24
W lobe					33			36 x 30
0149+35	01 49 50.0	35 54 20	0.0160	14.5	78			58
NGC 703								
core	01 49 50.0	35 54 20			15	2.4 x 1.7	(40)	
E jet					28			24 x 15
W jet					35			24 x 15
0206+35	02 06 39.3	35 33 41	0.0375	14.9	2050			89
4C35.03								
core	02 06 39.3	35 33 42			392	6.4 x 0.9	(131)	
E jet					210			37 x 12
W jet					262			28 x 12
halo					1186			89 x 51
0207+38	02 07 07.1	38 57 22	0.0181	13.0	98			34 x 19
NGC 828								
0222+36	02 22 23.9	36 56 57	0.0327	15.0				
core	02 22 23.9	36 56 57			199	0.8 x 0.5	(53)	
0258+35	02 58 35.6	35 00 31	0.0160	14.0				
NGC1167								
4C34.09								
core	02 58 35.4	35 00 32			1822	1.4 x 0.6	(117)	
0331+39	03 31 01.0	39 11 25	0.0202	14.2	904			68
4C39.12								
core	03 31 00.9	39 11 23			456	2.9 x 2.1	(165)	
halo					448			68 x 31
0648+27	06 48 54.9	27 31 18	0.0409	14.9				
core	06 48 54.8	27 31 18			156	0.8 x 0.4	(20)	
0722+30	07 22 27.5	30 03 14	0.0191	15.6	136			35 x 12
0800+24	08 00 16.3	24 49 02	0.0433	15.7	100			94
head					27			28 x 5
N tail					38			84 x 9
S tail					35			56 x 9
0836+29	08 36 59.1	29 59 45	0.0650	15.7	575			64
4C29.30								
core	08 36 58.9	29 59 40			40			
N lobe	59.4	53			160	4 x 3	(44)	
S lobe	58.3	24			170	4 x 3	(18)	
S diffuse					120			34 x 24
1040+31	10 40 31.0	31 46 45	0.0360	15.5	770			54
4C29.41								
core	10 40 31.1	31 46 49			25			
jet?					>20			
halo					725			54 x 42
1108+27	11 08 44.3	27 14 06	0.0331	14.6	87			72
core	11 08 44.0	27 14 07			16	< 2.0		
E jet					7			25 x 7
W jet					64			36 x 10
1113+29	11 13 53.4	29 31 34	0.0489	15.1	1810			91
4C29.41								
core	11 13 53.4	29 31 39			104	6.9 x 0.5	(78)	
E lobe					737			48 x 47
W lobe					546			44 x 31
W jet					300			
W hot-spot	11 13 51.3	29 31 35			124			
1122+39	11 22 01.4	39 02 19	0.0067	11.6	92			75
NGC3665								
core	11 22 01.2	39 02 16			20	5.8 x 1.9	(138)	
E jet					38			30 x 12
W jet					32			35 x 10

TABLE IIa (*continued*).

NAME	R.A. h m sec	DEC. ° ' "	z	m_{pg}	S(1.4) mJy	Size FWHM arcsec	P.A. deg.	LAS arcsec
1144+35	11 44 45.5	35 17 49	0.0630	15.7	556			25
core	11 44 45.5	35 17 47			529	0.5 x 0.4	(98)	
E jet					27			25 x 8
1254+27	12 54 59.4	27 46 02	0.0249	13.6	65			43
NGC4839								
N lobe					37			24 x 14
S lobe					28			17 x 14
1317+33	13 17 55.8	33 24 19	0.0379	15.0	78			28 x 15
NGC5098								
1318+34	13 18 16.9	34 23 56	0.0232	14.8				
core	13 18 17.0	34 24 04			95	2.5 x 1.2	(141)	
1322+36	13 22 35.4	36 38 19	0.0175	13.9	808			53
NGC5141								
4C36.24								
core	13 22 35.3	36 38 17			90	<7 x <1.5		
N lobe					329			22 x 22
S lobe					389			25 x 22
1346+26	13 46 34.1	26 50 28	0.0633	15.5	820			21 x 10
4C26.42								
1506+34	15 06 05.6	34 34 18	0.0452	15.6				
core	15 06 05.3	34 34 49			115	1.2 x 0.8	(54)	
1525+29	15 25 39.6	29 06 28	0.0653	15.4	216			32 x 17
1553+24	15 53 56.3	24 35 32	0.0426	15.4	119			61
core	15 53 56.1	24 35 33			62	3.1 x 0.5	(138)	
N jet					38			30 x 8
S jet					19			22 x 8
1610+29	16 10 36.6	29 36 52	0.0313	14.8	82			135
NGC6086								
E lobe					28			63 x 58
W lobe					54			77 x 39
1621+38	16 21 16.9	38 02 17	0.0310	14.1	395			57
NGC6137								
core	16 21 16.8	38 02 14			54	3.5 x 1.8	(3)	
N jet					24	3.5 x 2.8	(157)	
tail					317			57 x 22
1626+39	16 26 55.4	39 39 36	0.0303	13.9	3175			110
NGC6166								
3C338								
core	16 26 55.3	39 39 36			180	<2 x <1		
E lobe					1597			50 x 28
W lobe					1400			56 x 36
1652+39	16 52 11.8	39 50 25	0.0337	13.7				
4C39.49								
core	16 52 11.7	39 50 25			1382	0.5 x 0.5	(97)	
1833+32	18 33 12.0	32 39 18	0.0585	15.5	3217			170
3C382								
core	18 33 12.0	32 39 18			194	1.3 x 0.9	(59)	
E lobe					1434			90 x 36
W lobe					983			50 x 48
E hot-spot	18 33 18.0	32 39 58			526	4.7 x 4.1	(43)	
W hot-spot	07.2	25			80	3.4 x 3.5	(90)	
1855+37	18 55 54.3	37 56 27	0.0552	14.9	362	6.9 x 2.7	(15)	
2116+26	21 16 20.7	26 14 08	0.0164	14.0	105			78
core	21 16 20.8	26 14 08			56	3.2 x 1.0	(22)	
N jet					16			33 x 7
S jet					25			34 x 10
2236+35	22 36 12.3	35 04 11	0.0277	15.0	348			47
core	22 36 12.3	35 04 10			6			
E lobe					93			35 x 23
W lobe					76			31 x 22
E jet					85			19 x 7
W jet					94			22 x 9

TABLE IIb. — *Observational data.*

NAME	R.A. h m sec	DEC. ° ' "	z	m_v	S(1.4) mJy	Size FWHM arcsec	Size P.A. deg.	LAS arcsec
0708+32	07 08 33.6	32 23 37	0.0672	15.8	56			14 x 7
0908+37	09 08 45.4	37 36 33	0.1040	15.5	626			51
core	09 08 45.3	37 36 33			35	< 2.0		
N lobe					290			23 x 23
S lobe					302			27 x 21
0913+38	09 13 39.1	38 30 41	0.0711	15.7	346			47
E lobe					160			26 x 21
W lobe					190			28 x 21
1003+26	10 03 49.4	26 09 24	0.1165	16.5				
core	10 03 49.4	26 09 23			71	3.9 x 1.5	(8)	
1037+30	10 37 42.7	30 13 38	0.0908	16.4				
core	10 37 42.8	30 13 38			390	1.9 x 0.4	(140)	
1113+24	11 13 24.0	24 57 24	0.1021	15.0	38			40
main comp.					25			18 x 13
N arc					13			39 x 10
1204+24	12 04 34.3	24 11 06	0.0769	15.2	128			33
core	12 04 34.4	24 11 07			24			
N lobe					23			8 x 6
S lobe					68			12 x 10
halo					13			33 x 18
1204+34	12 05 00.5	34 09 21	0.0788	15.8	413			62
core	12 05 00.4	34 09 21			20	1.4 x 1.3	(119)	
E lobe					200			32 x 32
W lobe					146			28 x 28
W hot-spot	12 04 58.7	34 09 38			47	< 2.0		
1303+31	13 03 28.3	31 10 20	0.1816	16.7	67			19 x 9
1339+26								
head tail	13 39 30.7	26 37 20	0.0757	14.2	242			>35 x 11
WAT	29.4	35	0.0688	14.2	23			24 x 7
1347+28	13 47 56.3	28 31 34	0.0724	15.2	198			54
core	13 47 56.4	28 31 35			10	< 2.0		
E lobe					98			24 x 22
W lobe					93			28 x 26
1358+28	13 58 51.3	28 54 55	0.0823	15.1	248			25
E lobe					150			15 x 6
W lobe					98			11 x 6
1430+25	14 30 26.9	25 08 28	0.0813	15.7	537			71
N comp	14 30 27.0	25 08 34			150			
head					309			23 x 8
tail					78			27 x 6
1450+28	14 50 23.8	28 10 05	0.1265	16.5	125			57
E lobe					67			28 x 25
W lobe					39			28 x 25
1527+30	15 27 43.3	30 52 49	0.1143	15.0	81			73
core	15 27 43.3	30 52 50			24	3.4 x 1.8	(63)	
E tail					27			34 x 10
W tail					33			31 x 7
1557+26	15 57 45.9	26 04 51	0.0442	14.3				
core	15 57 46.0	26 04 51			31	2.3 x 1.1	(64)	
W source	44.0	58			118	0.8 x 0.3	(102)	
1609+31	16 09 42.3	31 10 41	0.0944	15.6	141			33
N lobe					79			18 x 16
S lobe					62			18 x 16

TABLE IIb (continued)

NAME	R.A. h m sec	DEC. ° ′ ″	z	m_v	S(1.4) mJy	Size FWHM arcsec	Size P.A. deg.	LAS arcsec
1613+27	16 13 28.9	27 34 21	0.0647	14.9	237			39
E lobe					126			24 x 17
W lobe					147			19 x 17
1638+32	16 38 34.9	32 11 09	0.1398	15.8	309			57
core	16 38 34.9	32 11 10			106	2.3 x 1.9	(104)	
tail					203			57 x 22
1658+32	16 58 18.7	32 39 37	0.102	16.1	110			54
head	16 58 18.6	32 39 32			45	14 x 4	(4)	
tail					65			54 x 13
1736+32	17 36 45.2	32 57 36	0.0741	15.1	223			44
E comp					105			17 x 19
C comp					25			
W comp					90			15 x 13
1747+30	17 47 56.3	30 18 55	0.1297	16.7	49			98
core	17 47 56.3	30 18 56			7			
S lobe					29			43 x 20
N jet					13			54 x <2
1752+32	17 52 44.5	32 34 45	0.0449	14.3	136			95
core	17 52 44.4	32 34 44			20	~ 4		
E jet					35			37 x 9
W jet					65			50 x 12

TABLE IIIa. — *Intrinsic properties.*

NAME	z	M_{pg}	log $P_{1.4}$ W/Hz	linear resolution kpc	Linear size kpc	u_{min} E-12 erg/cm^3	H_{eq} micro gauss
0120+33	0.0164	-20.7	22.30	0.8 x 0.8	23		
NGC 507							
E lobe					9 x 6	1.5	4.0
W lobe					9 x 7	1.5	4.0
0149+35	0.0160	-19.1	22.33	0.9 x 0.8	14		
NGC 703							
core					0.6 x 0.4		
E jet					5.6 x 3.5	4.0	6.0
W jet					5.6 x 3.5	4.0	7.0
0206+35	0.0375	-20.7	24.50	1.8 x 1.8	47		
4C35.03							
core					3.3 x 0.5		
E jet					19 x 6	8	9.0
W jet					15 x 6	11	11.0
halo					46 x 27	2.5	5.0
0207+38	0.0181	-21.0	22.54	0.9 x 0.9	9 x 5	4.5	7.0
NGC 828							
0222+36	0.0327	-20.3	23.36	1.5 x 1.3			
core					0.4 x 0.2		
0258+35	0.0160	-19.8	23.67	0.8 x 0.7			
NGC1167							
4C34.09							
core					0.3 x 0.1		
0331+39	0.0202	-20.5	23.60	1.1 x 0.9	20		
4C39.12							
core					0.8 x 0.6		
halo					20 x 9	4.0	6.5
0648+27	0.0409	-21.3	23.62	2.0 x 1.8			
core					0.4 x 0.2		
0722+30	0.0191	-18.6	22.67	0.9 x 0.9	10 x 3	9.0	10.0
0800+24	0.0433	-20.1	23.30	2.3 x 2.3	56		
head					17 x 3	7.5	9.0
N tail					50 x 5	2.5	5.0
S tail					33 x 5	3.0	6.0
0836+29	0.0650	-20.9	24.41	3.7 x 3.2	55		
4C29.30							
N lobe					3.4 x 2.6	95	32
S lobe					3.4 x 2.6	98	32
S diffuse					29 x 21	2.0	5.0
1040+31	0.0360	-19.6	24.03	2.0 x 1.7	27		
4C29.41							
halo					27 x 21	3.0	6.0
1108+27	0.0331	-20.3	23.01	1.7 x 1.5	33		
E jet					12 x 3	3.0	5.5
W jet					17 x 5	5.5	7.5
1113+29	0.0489	-20.7	24.67	2.5 x 2.3	61		
4C29.41							
core					4.6 x 0.3		
E lobe					32 x 31	2.5	5.5
W lobe					29 x 21	4.0	6.5
1122+39	0.0067	-19.9	21.65	0.3 x 0.3	7		
NGC3665							
core					0.6 x 0.2		
E jet					3.0 x 1.0	8.0	9.5
W jet					3.5 x 1.0	8.5	9.5
1144+35	0.0630	-20.7	24.35	2.9 x 2.7	21		
core					0.4 x 0.3		
E jet					21 x 7	4.0	6.5

TABLE IIIa (continued)

NAME	z	M_{pg}	log $P_{1.4}$ W/Hz	linear resolution kpc	Linear size kpc	u_{min} E-12 erg/cm^3	H_{eq} micro gauss
1254+27	0.0249	-20.6	22.63	1.4 x 1.2	15		
NGC4839							
N lobe					8.5 x 5.0	4.0	6.5
S lobe					6.0 x 5.0	4.0	6.5
1317+33	0.0379	-20.3	23.08	1.7 x 1.7	15 x 8	4.0	6.5
NGC5098							
1318+34	0.0232	-19.3	22.74	1.4 x 1.4			
core					0.8 x 0.4		
1322+36	0.0175	-19.6	23.42	1.0 x 1.0	13		
NGC5141							
4C36.24							
N lobe					6 x 6	10.0	10.5
S lobe					6 x 6	10.5	10.0
1346+26	0.0633	-20.9	24.55	2.8 x 2.5	18 x 8	24.0	16.0
4C26.42							
1506+34	0.0452	-20.0	23.40	2.4 x 2.4			
core					0.7 x 0.5		
1525+29	0.0653	-21.0	23.98	3.1 x 2.8	28 x 15	4.5	7.0
1553+24	0.0426	-20.1	23.36	2.0 x 1.9	36		
core					1.8 x 0.3		
N jet					18 x 5	5.0	7.5
S jet					13 x 5	4.0	6.5
1610+29	0.0313	-20.1	22.93	2.9 x 2.1	60		
NGC6086							
E lobe					28 x 26	0.5	2.0
W lobe					34 x 17xx	1.0	3.0
1621+38	0.0310	-20.8	23.65	2.9 x 2.8	25		
NGC6137							
core					1.5 x 0.8		
N jet					1.5 x 1.2	52	24
tail					25 x 1	4.5	7.0
1626+39	0.0303	-21.1	24.49	1.7 x 1.7	47		
NGC6166							
3C338							
E lobe					21 x 12	9.0	10.0
W lobe					24 x 15	6.0	8.0
1652+39	0.0337	-21.4	24.23	1.8 x 1.7			
4C39.49							
core					0.2 x 0.2		
1833+32	0.0585	-21.0	25.07	2.6 x 2.6	133		
3C382							
core					1.0 x 0.7		
E lobe					70 x 28	3.5	6.0
W lobe					39 x 38	2.5	5.5
E hot-spot					3.7 x 3.2	120	36
W hot-spot					2.7 x 2.7	61	26
1855+37	0.0552	-21.8	24.07	2.9 x 2.5	5.1 x 2.0	130	38
2116+26	0.0164	-20.0	22.48	0.9 x 0.8	19		
core					0.8 x 0.2		
N jet					8 x 1.5	5.5	7.5
S jet					8 x 2.5	4.5	7.0
2236+35	0.0277	-19.9	23.47	1.2 x 1.2	19		
E lobe					14 x 9	3.0	5.5
W lobe					12 x 9	3.0	5.5
E jet					8 x 3	15	13
W jet					9 x 3	11	11

1986A&AS...64..135P

TABLE IIIb. — *Intrinsic properties.*

NAME	z	M_v	log $P_{1.4}$ W/Hz	linear resolution kpc	Linear size kpc	u_{min} E-12 erg/cm^3	H_{eq} micro gauss
0708+32	0.0672	-21.2	23.51	2.8 x 2.6	120 x 6	9.5	10
0908+37	0.1040	-22.2	24.84	4.4 x 4.2	65		
N lobe					29 x 29	4.0	6.5
S lobe					35 x 27	4.5	7.0
0913+38	0.0711	-21.1	24.27	3.1 x 2.7	44		
E lobe					24 x 20	3.5	6.0
W lobe					26 x 20	3.0	6.0
1003+26	0.1165	-21.3	24.01	4.9 x 4.7			
core					5.5 x 2.1		
1037+30	0.0908	-20.9	24.51	4.2 x 3.8			
core					2.2 x 0.5		
1113+24	0.1021	-22.5	23.65	4.4 x 4.3	50		
main comp.					23 x 16	2.5	5.0
N arc					43 x 13	1.5	4.0
1204+24	0.0769	-21.7	23.91	3.3 x 3.0	33		
N lobe					8 x 6	9.0	10.0
S lobe					12 x 10	7.5	9.0
halo					33 x 18	1.0	3.0
1204+34	0.0788	-21.2	24.47	3.4 x 2.9	63		
core					1.4 x 1.3		
E lobe					32 x 32	2.0	5.0
W lobe					28 x 28	2.0	5.0
1303+31	0.1816	-22.3	24.39	6.7 x 6.3	37 x 18	5.5	7.5
1339+26	0.0757			3.5 x 3.2			
head tail		-22.6	24.17		>34 x 11	7.5	9.0
WAT		-22.6	23.00		24 x 7	4.0	6.5
1347+28	0.0724	-21.6	24.05	3.3 x 3.2	51		
E lobe					23 x 21	2.5	5.5
W lobe					26 x 25	2.0	4.5
1358+28	0.0823	-22.0	24.22	4.4 x 4.2	26		
E lobe					16 x 6	18	14
W lobe					12 x 6	17	13
1430+25	0.0813	-21.3	24.58	4.0 x 3.9	74		
head					24 x 8	15	13
tail					28 x 6	9.0	10.0
1450+28	0.1265	-21.6	24.33	5.0 x 4.4	85		
E tail					42 x 37	1.5	4.0
W tail					42 x 37	1.0	3.5
1527+30	0.1143	-22.8	24.05	4.7 x 4.6	101		
core					4.7 x 2.5		
E tail					47 x 14	2.0	5.0
W tail					43 x 10	4.0	6.5
1557+26	0.0442	-21.4	22.81	2.2 x 2.1			
core					1.4 x 0.7		
1609+31	0.0944	-21.8	24.14	4.4 x 4.4	39		
N lobe					21 x 19	3.5	6.0
S lobe					21 x 19	3.0	6.0
1613+27	0.0647	-21.7	24.03	3.2 x 3.2	33		
E lobe					21 x 15	4.0	6.5
W lobe					16 x 15	5.0	7.5
1638+32	0.1398	-22.6	24.80	6.9 x 6.4	92		
core					3.7 x 3.1		
tail					92 x 36	2.0	4.5
1658+32	0.102	-21.6	24.09	5.3 x 5.2	68		
head					18 x 5	14	12
tail					68 x 16	2.0	4.5

TABLE IIIb *(continued)*

NAME	z	M_v	log $P_{1.4}$ W/Hz	linear resolution kpc	Linear size kpc	u_{min} E-12 erg/cm^3	H_{eq} micro gauss
1736+32	0.0741	-21.8	24.14	4.0 x 3.6	42		
E comp					16 x 15	4.5	7.0
W comp					15 x 13	5.5	8.0
1747+30	0.1297	-21.6	23.96	6.9 x 6.7	149		
S lobe					66 x 31	1.0	3.0
N jet					82 x <3	6.5	8.5
1752+32	0.0449	-21.6	23.47	2.2 x 2.1	59		
E jet					23 x 6	3.5	6.5
W jet					31 x 7	3.0	6.0

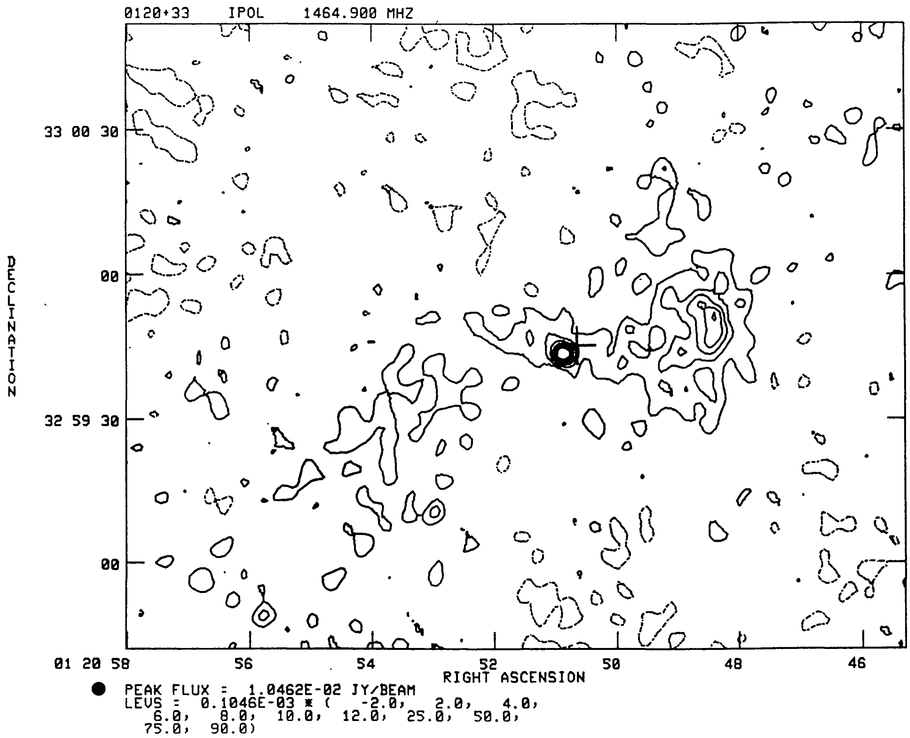

FIGURE 1a (1)

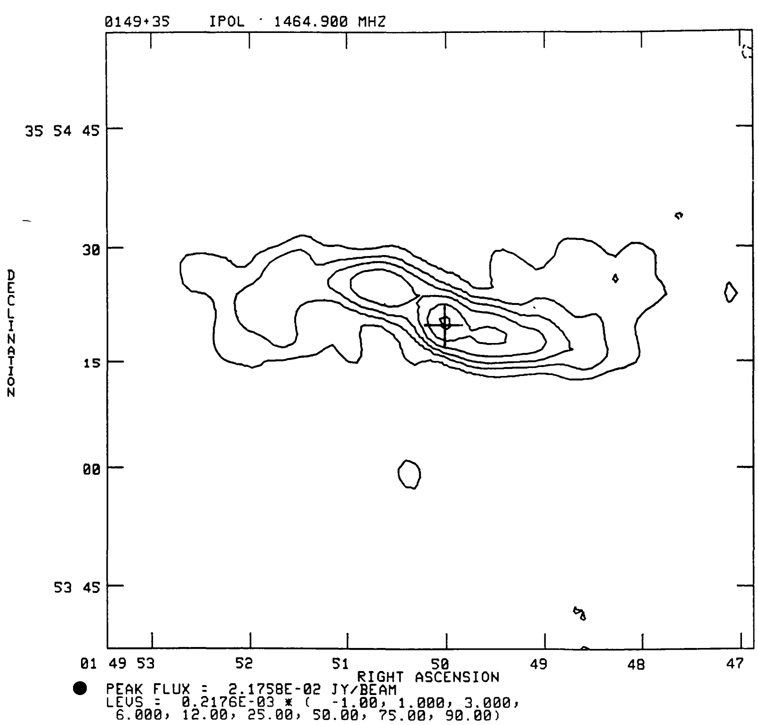

FIGURE 1a (2)

FIGURE 1a. — Contour maps of the resolved radiogalaxies from the « bright » sample (see text). The restoring beam is about 3.5 arsec. Levels are in mJy/beam. A black dot denotes the peak flux density of a source outside the mapped field. The cross marks the position of the optical identification.

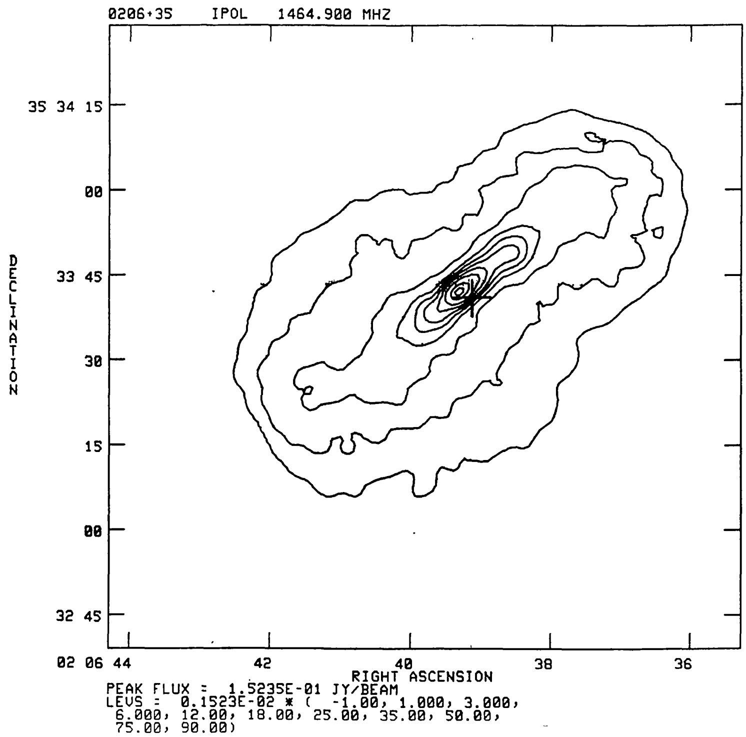

FIGURE 1a (3)

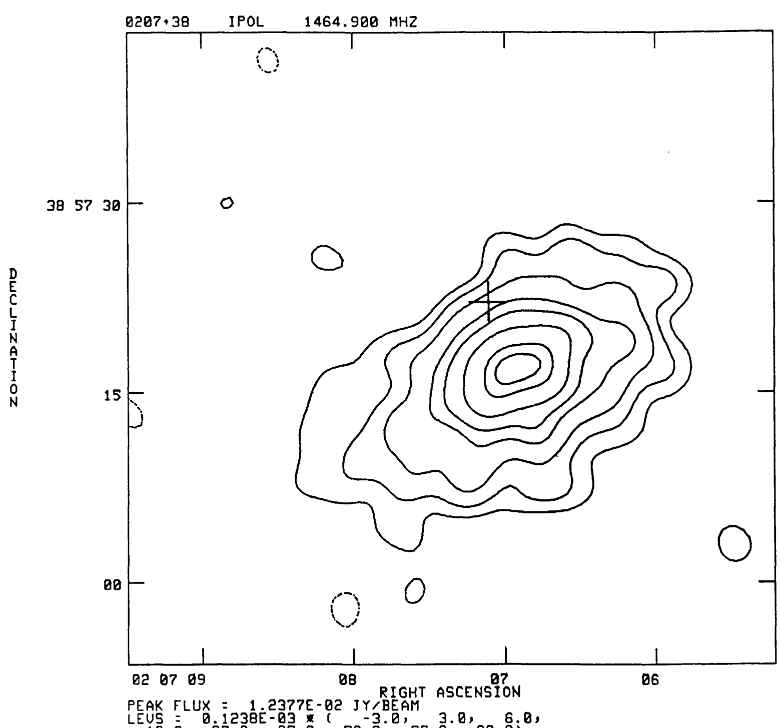

FIGURE 1a (4)

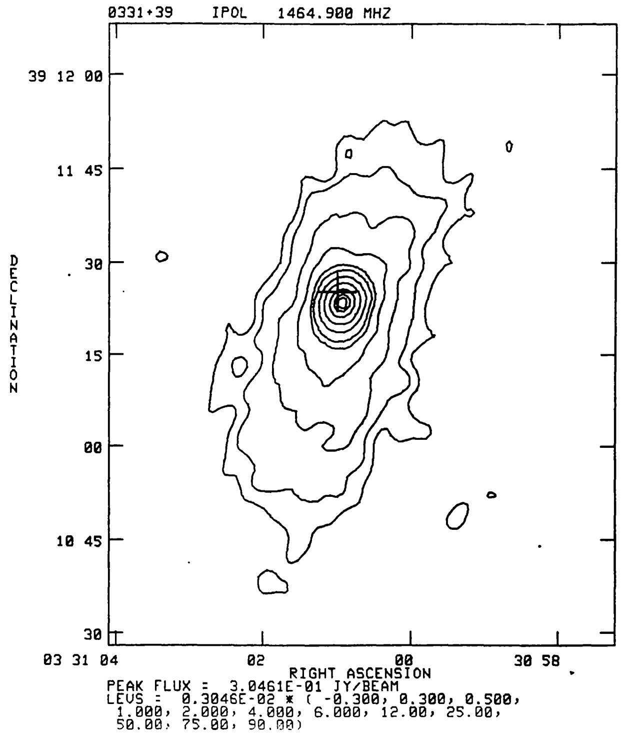

FIGURE 1a (5)

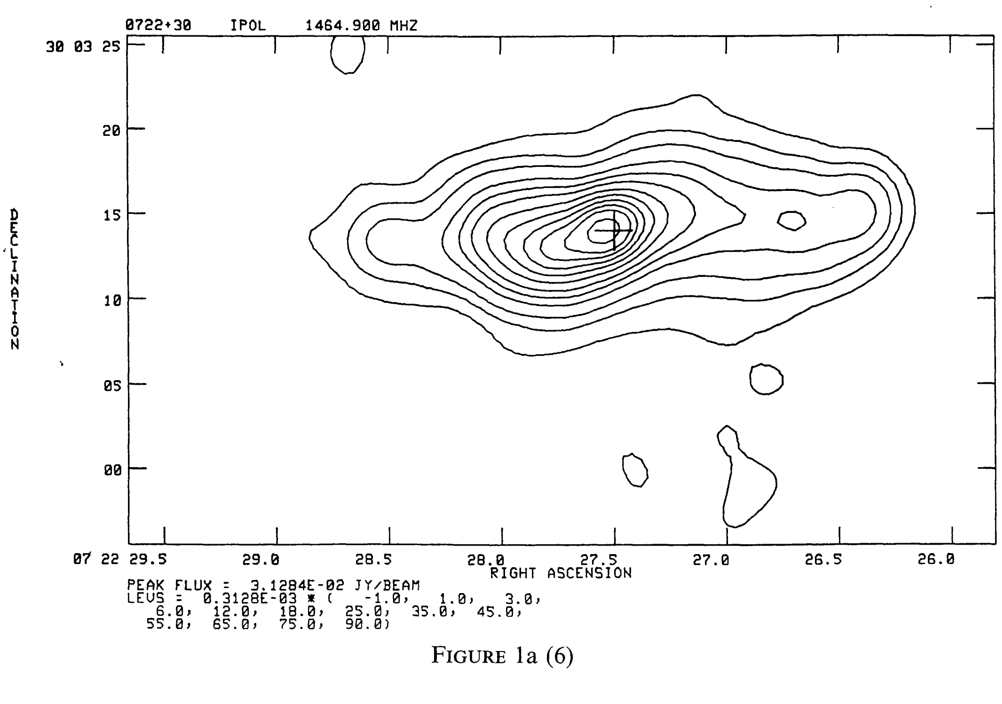

FIGURE 1a (6)

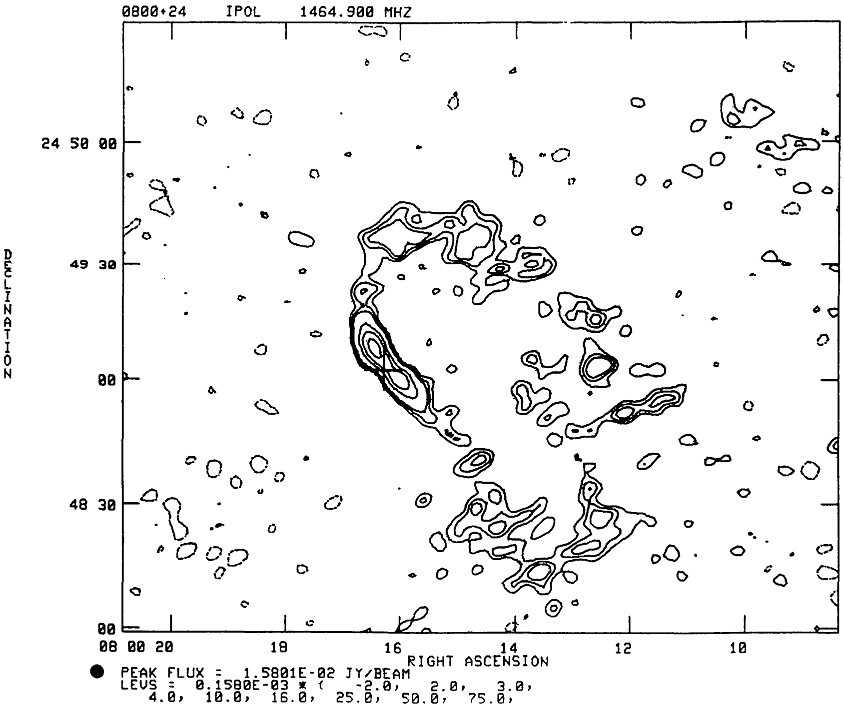

FIGURE 1a (7)

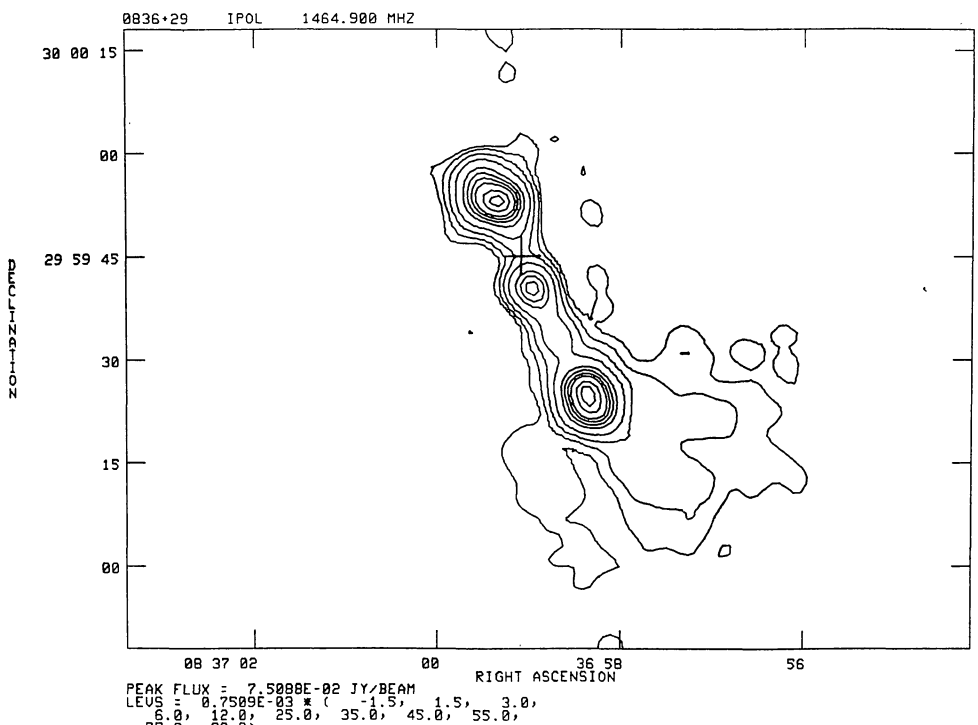

FIGURE 1a (8)

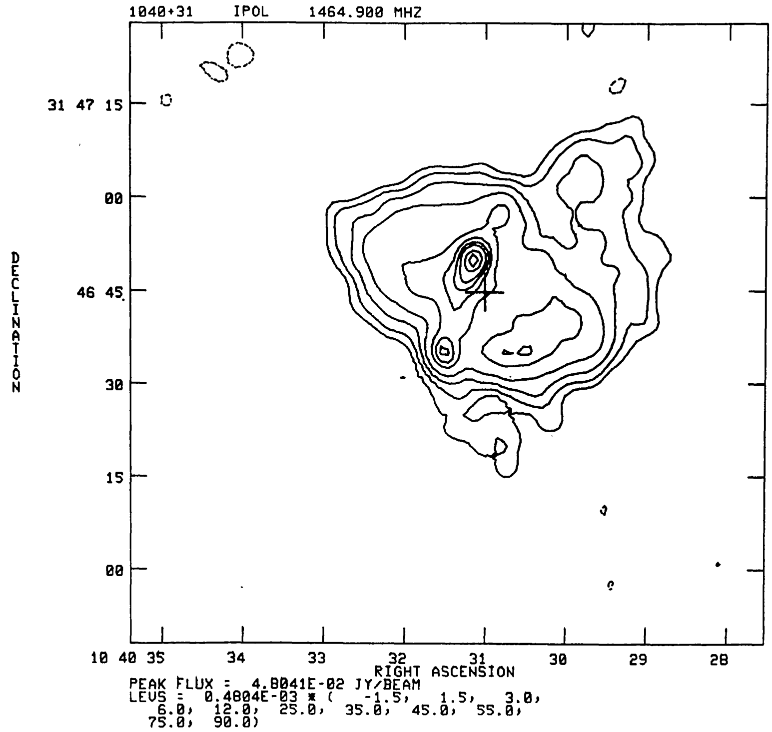

FIGURE 1a (9)

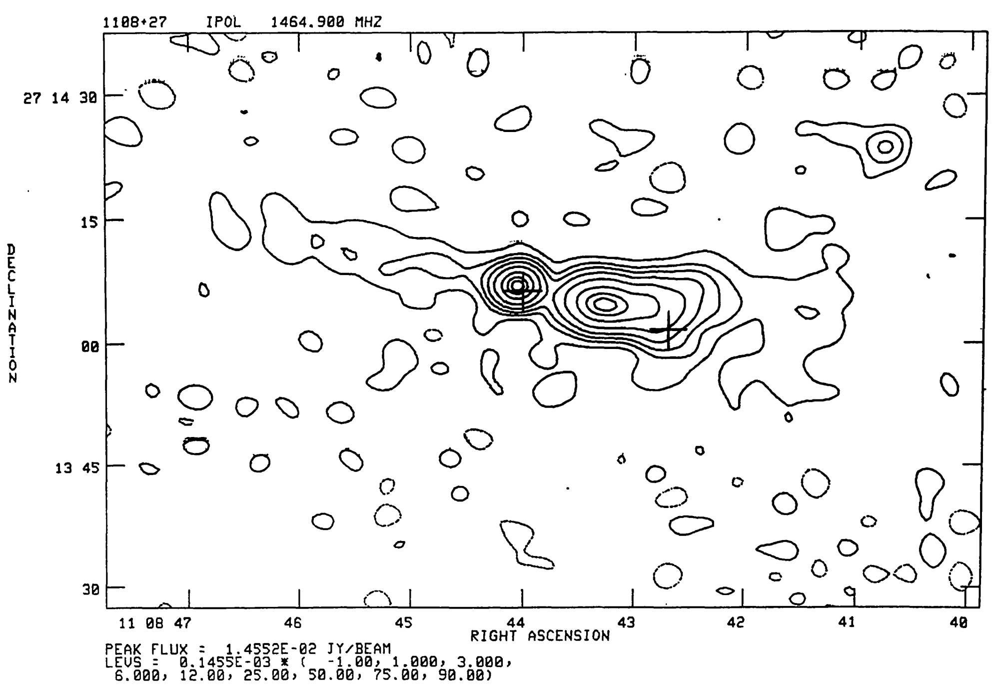

FIGURE 1a (10)

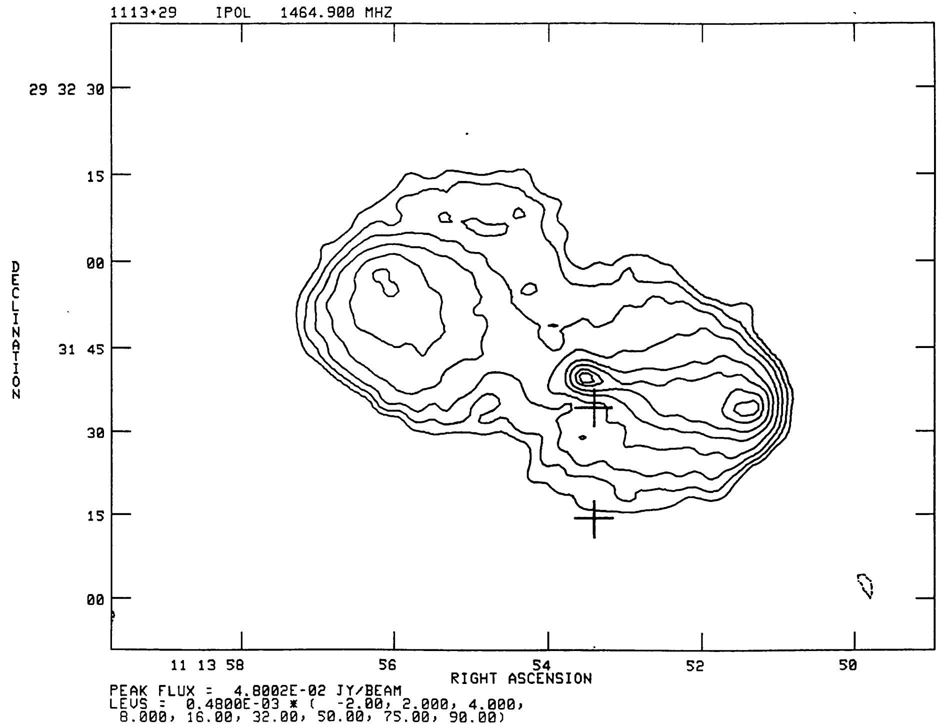

FIGURE 1a (11)

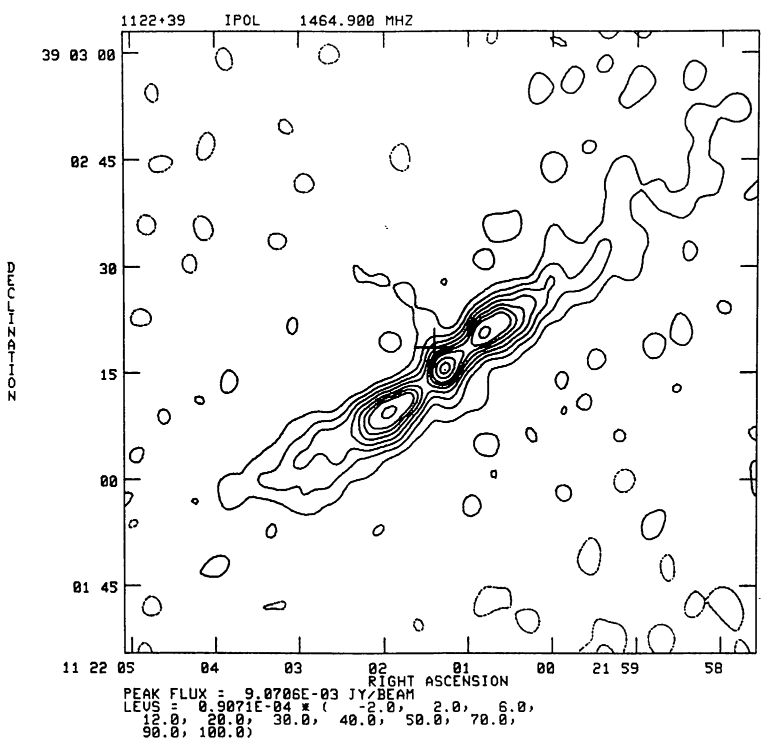

FIGURE 1a (12)

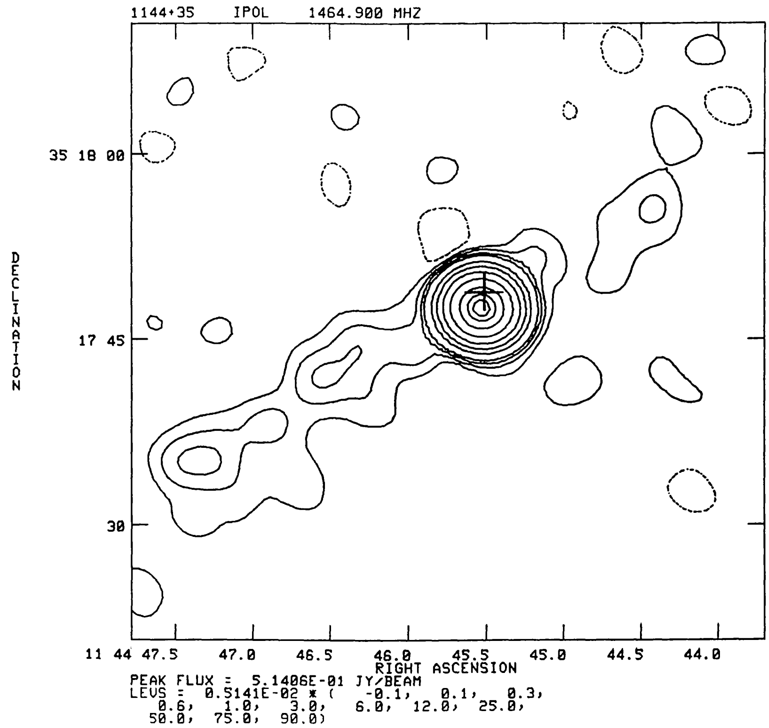

FIGURE 1a (13)

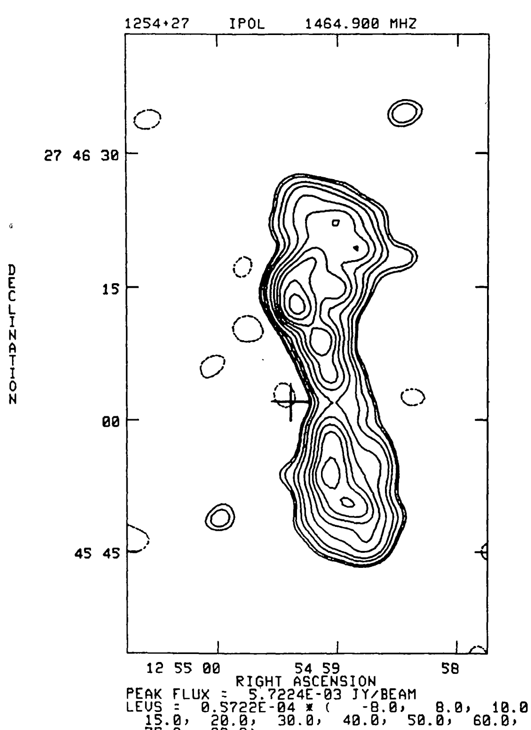

FIGURE 1a (14)

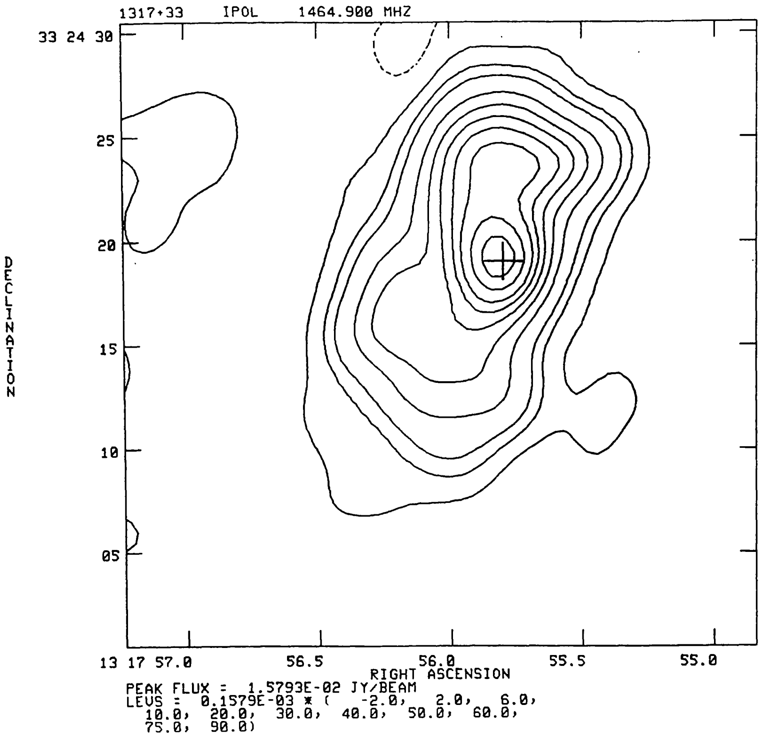

FIGURE 1a (15)

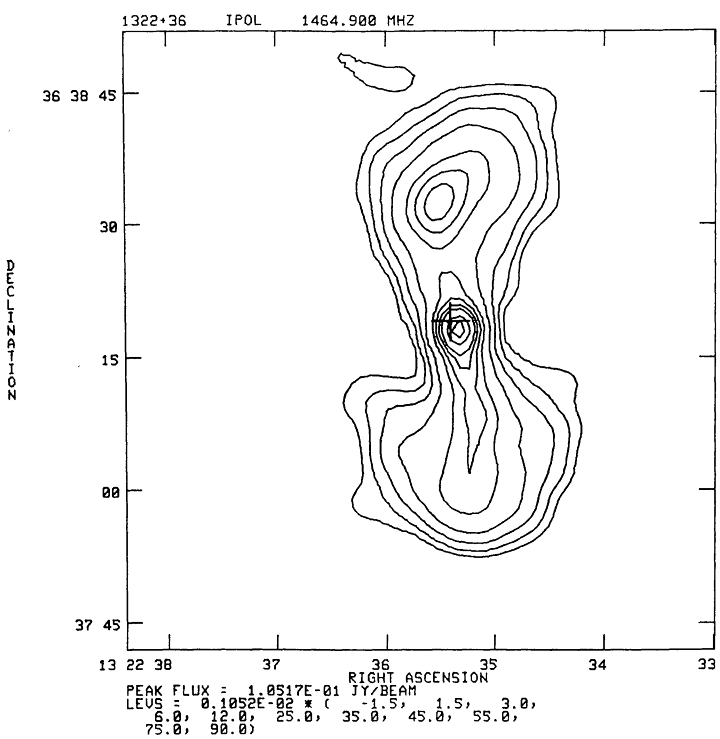

FIGURE 1a (16)

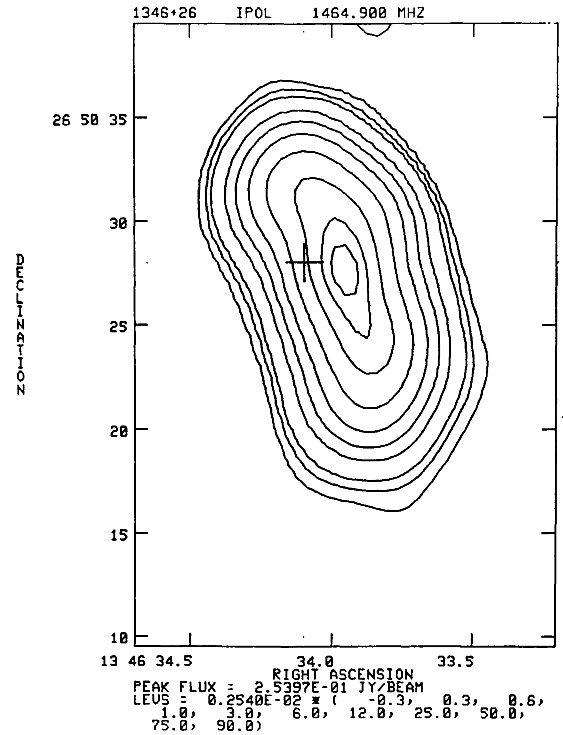

FIGURE 1a (17)

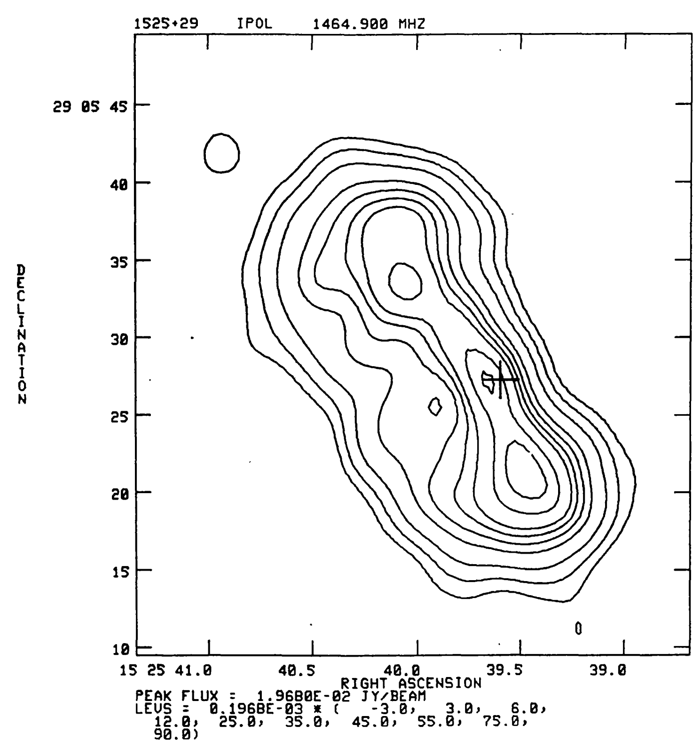

FIGURE 1a (18)

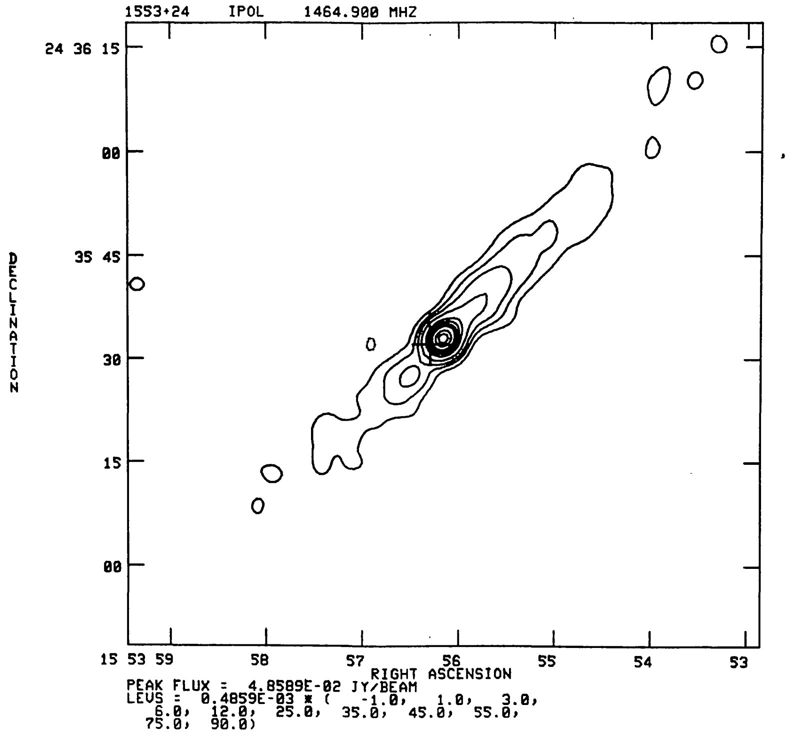

FIGURE 1a (19)

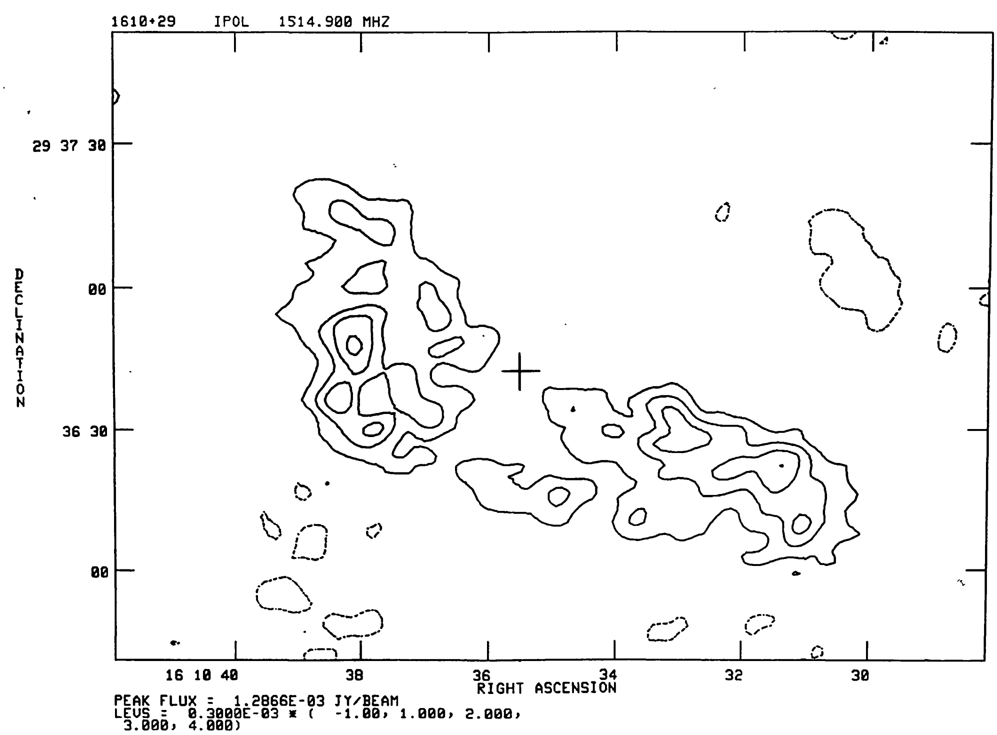

FIGURE 1a (20)

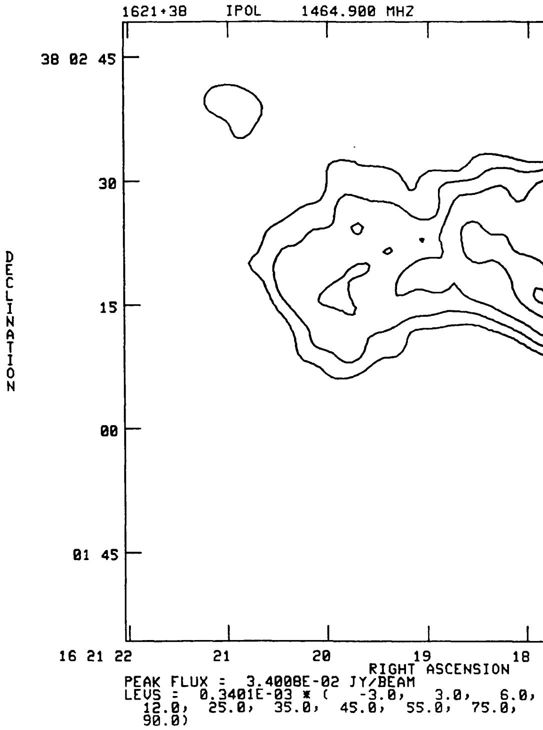

FIGURE 1a (21)

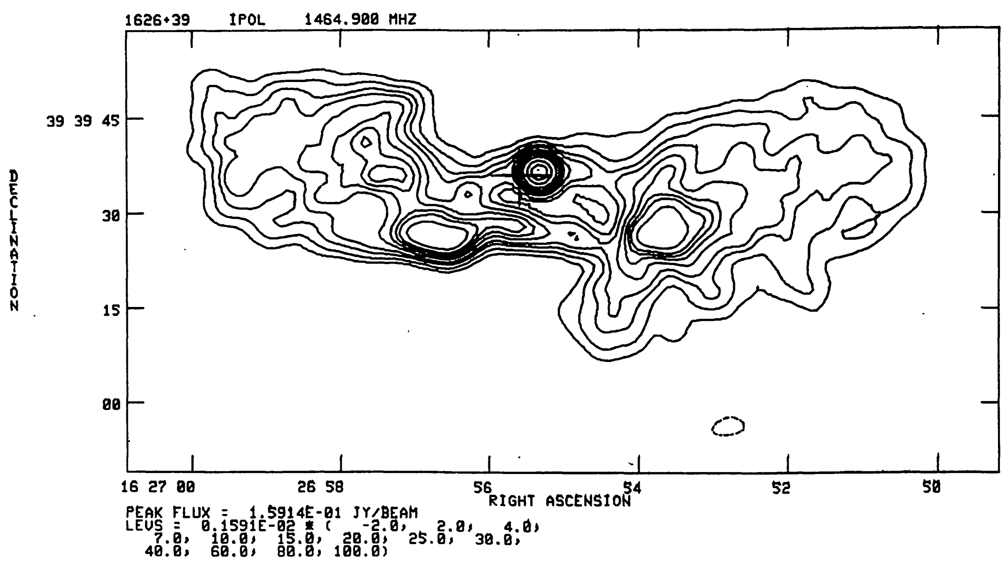

FIGURE 1a (22)

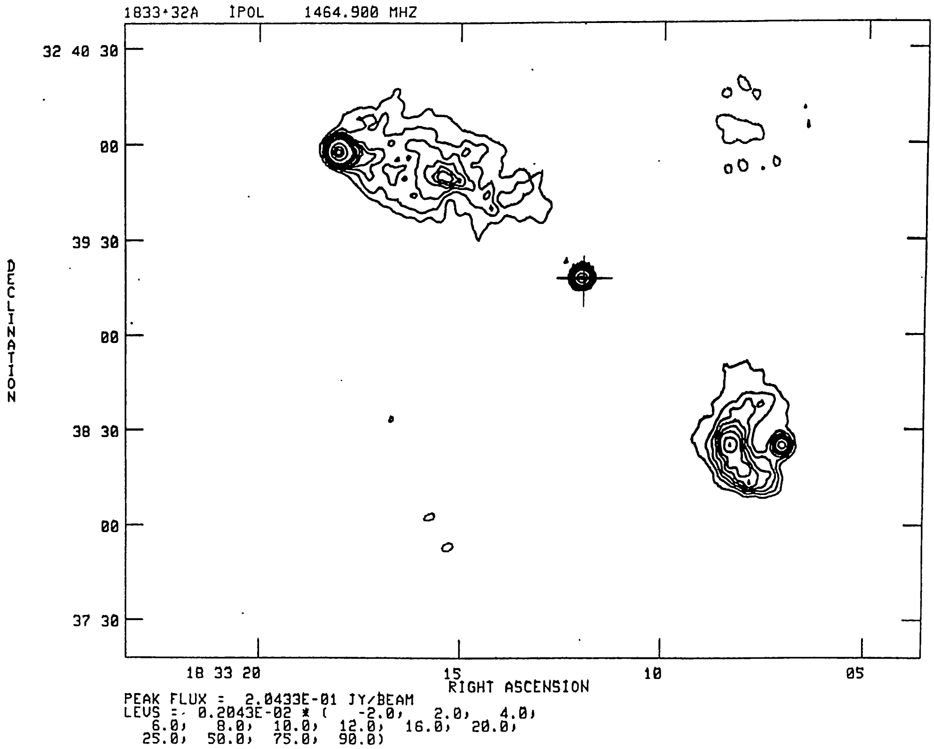

FIGURE 1a (23)

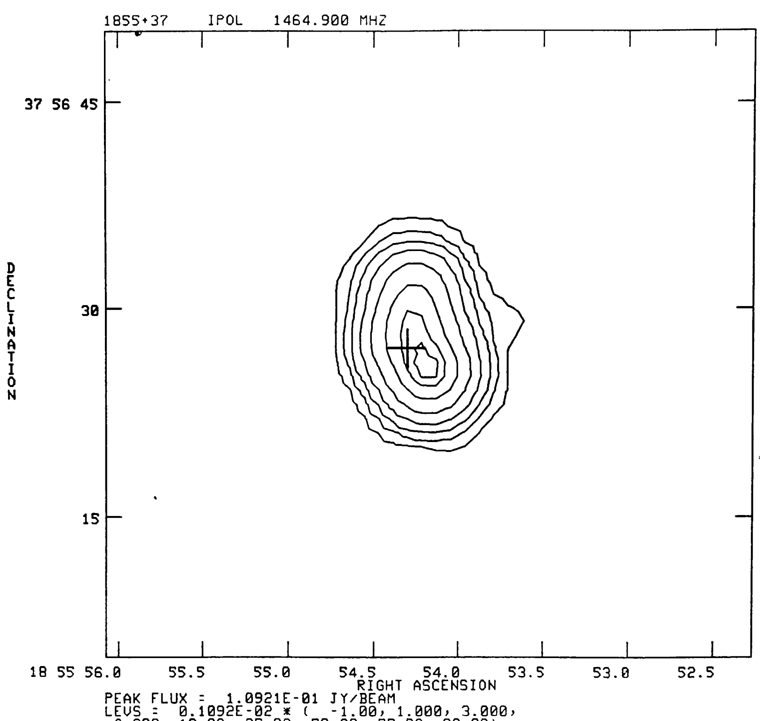

FIGURE 1a (24)

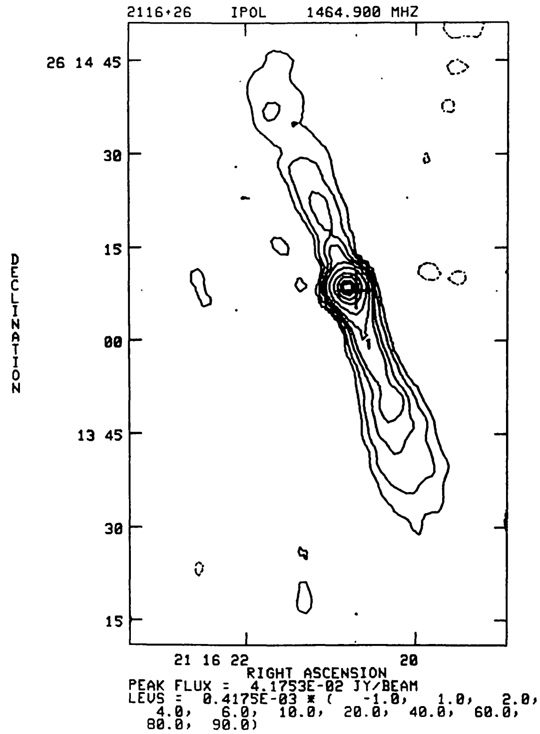

FIGURE 1a (25)

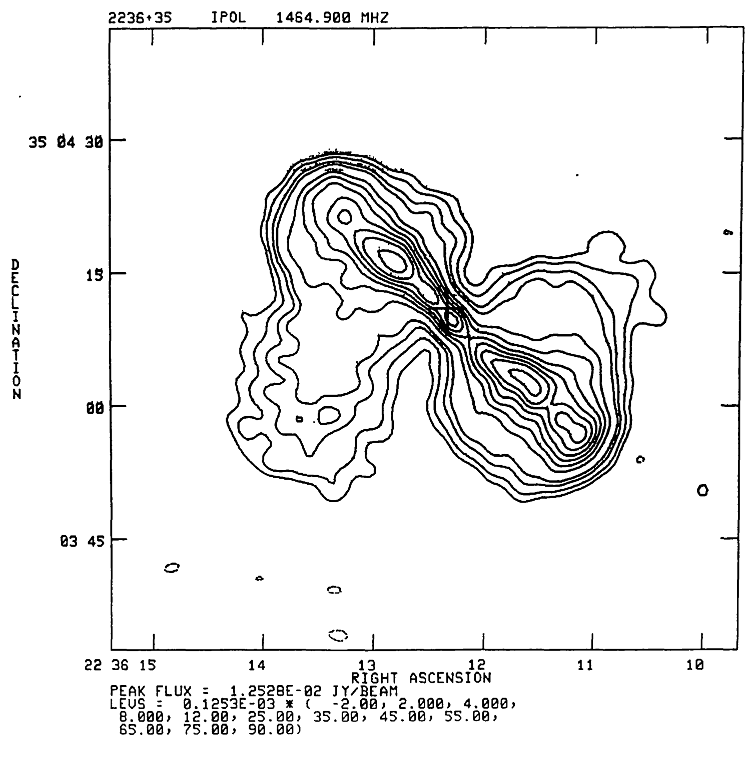

FIGURE 1a (26)

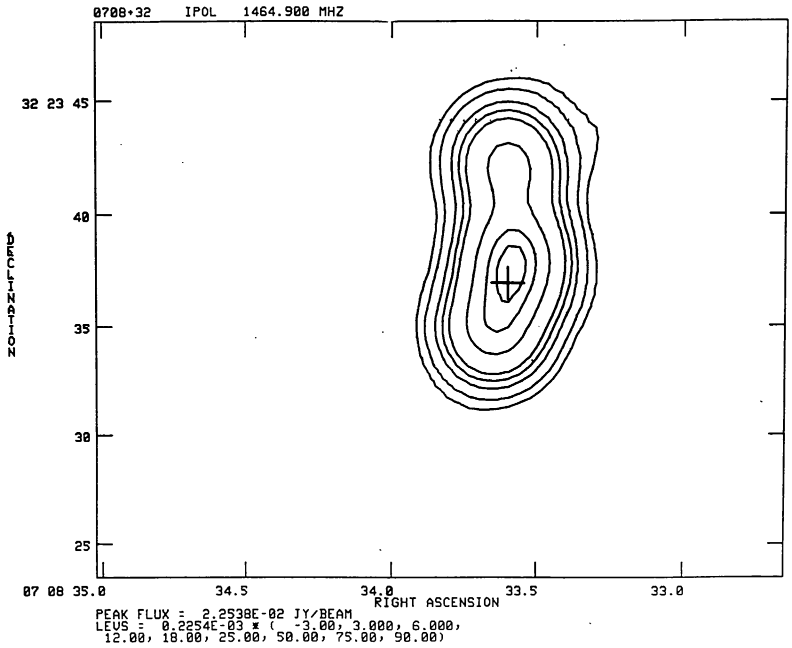

FIGURE 1b (1)

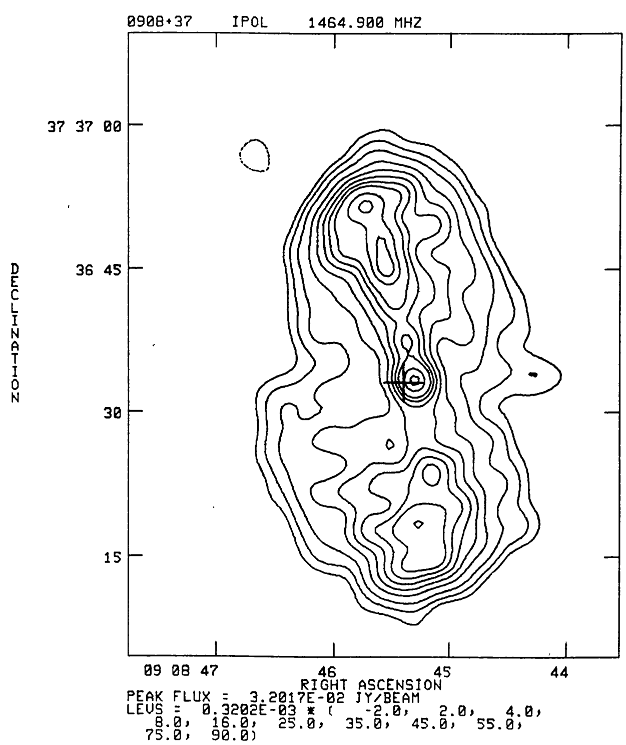

FIGURE 1b (2)

FIGURE 1b. — Contour maps of the resolved radiogalaxies from the « faint » sample (see text). The restoring beam is about 3.5 arcsec. Levels are in mJy/beam. A black dot denotes the peak flux density of a source outside the mapped field. The cross marks the position of the optical identification.

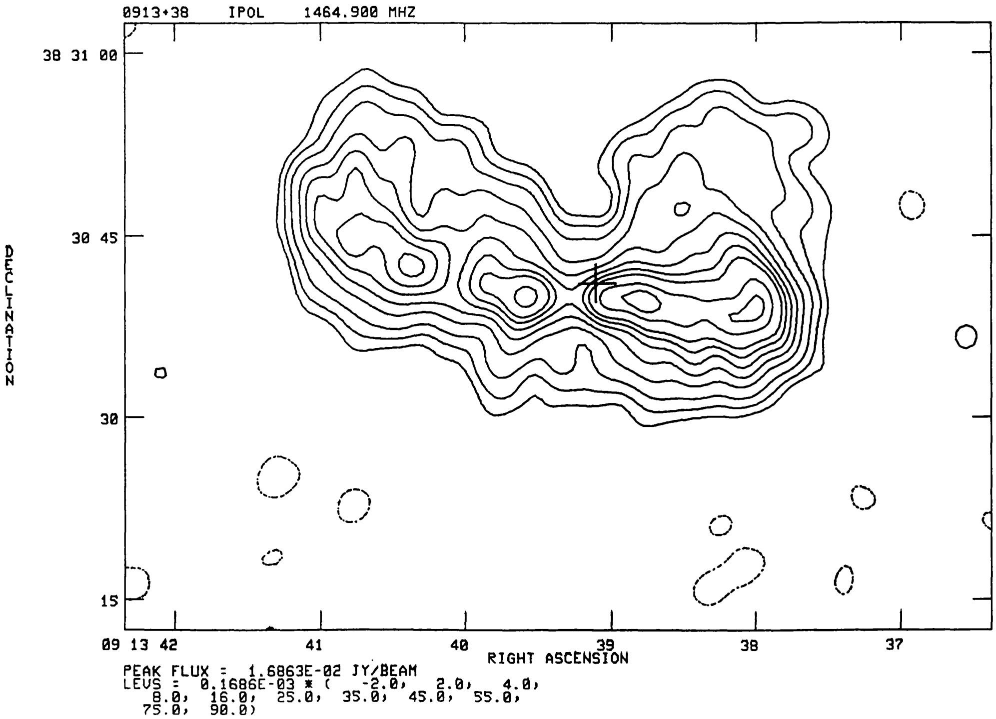

FIGURE 1b (3)

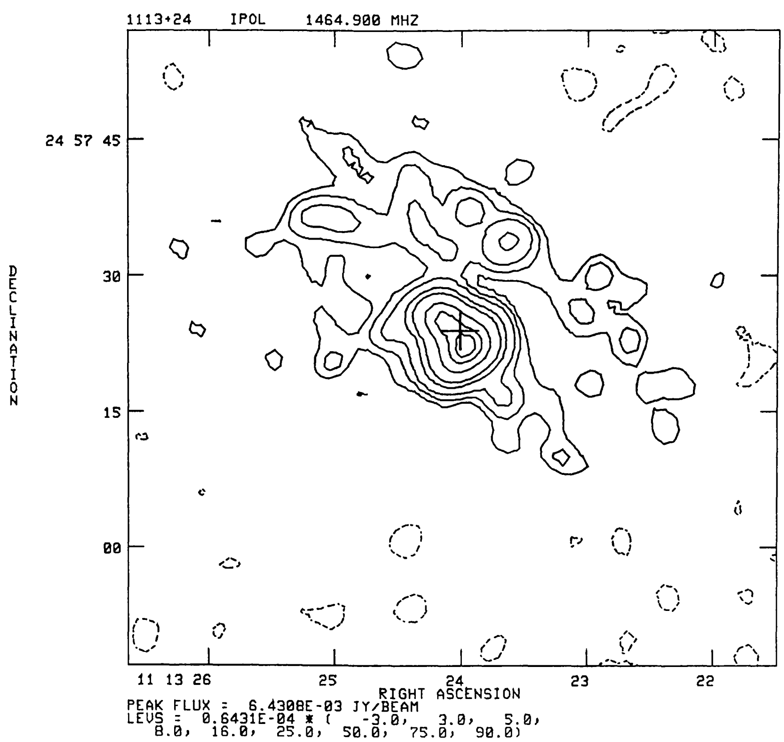

FIGURE 1b (4)

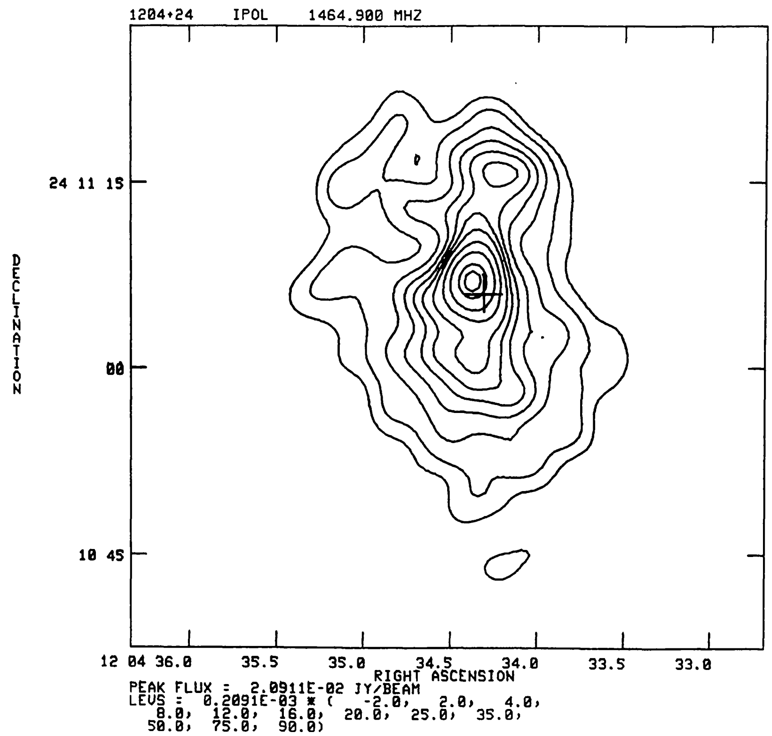

FIGURE 1b (5)

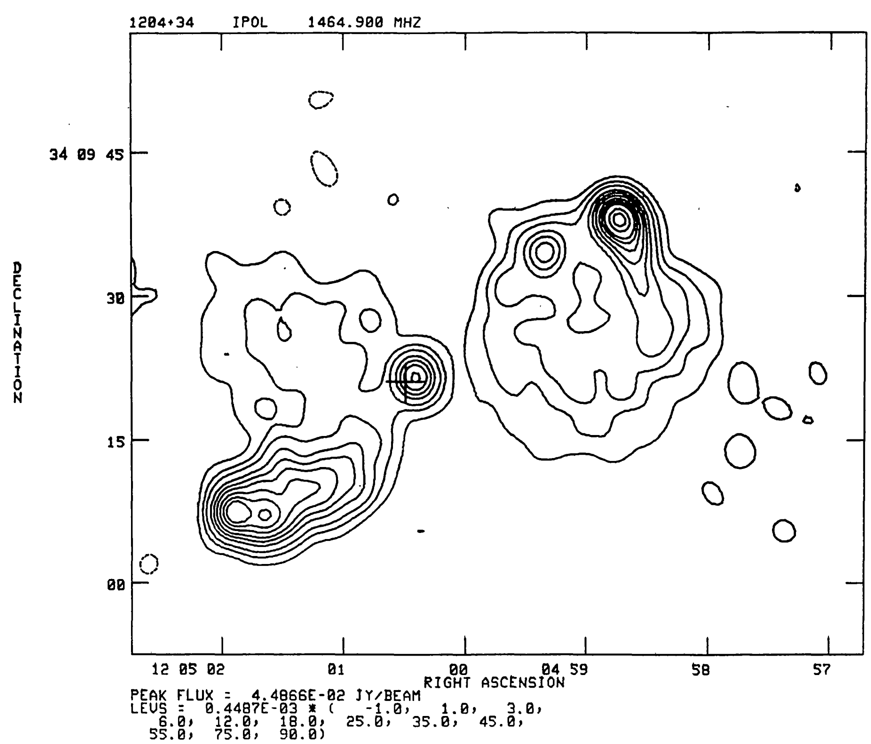

FIGURE 1b (6)

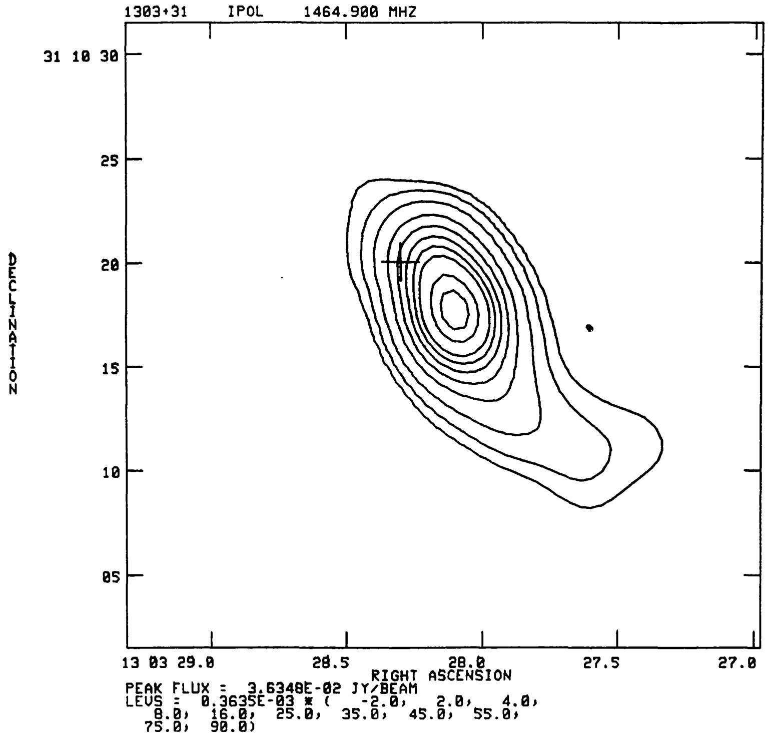

FIGURE 1b (7)

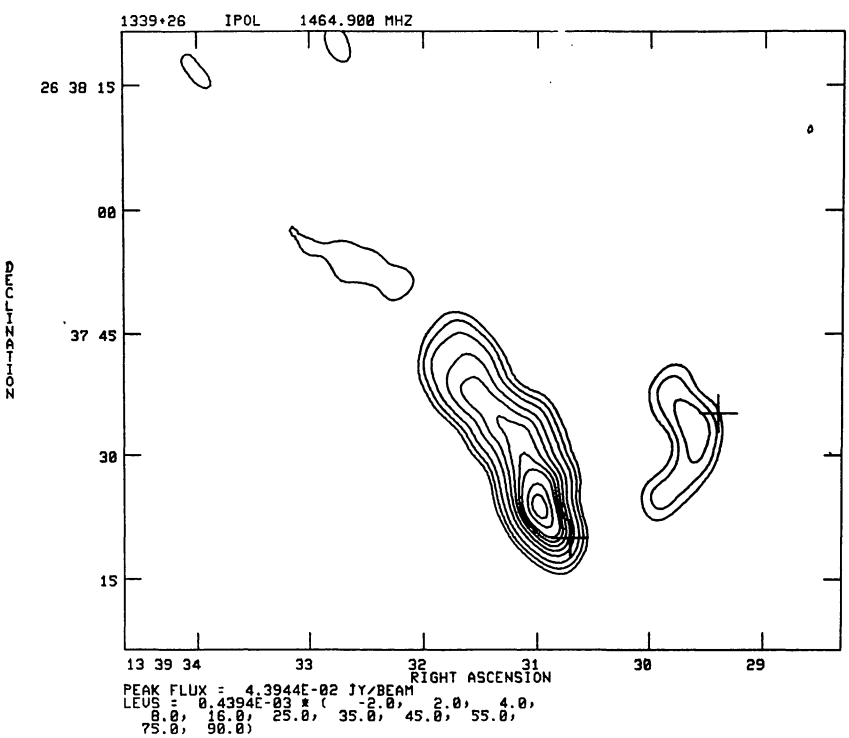

FIGURE 1b (8)

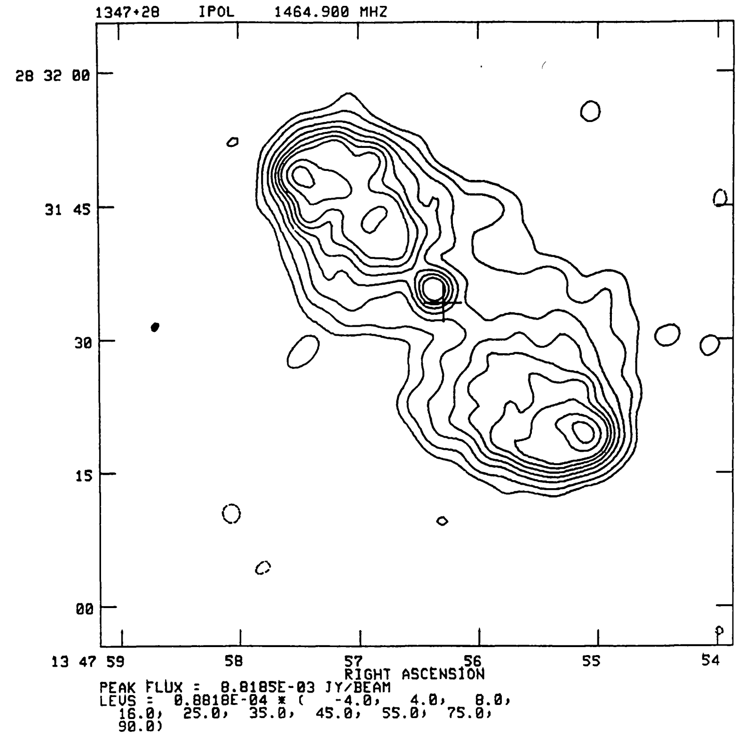

FIGURE 1b (9)

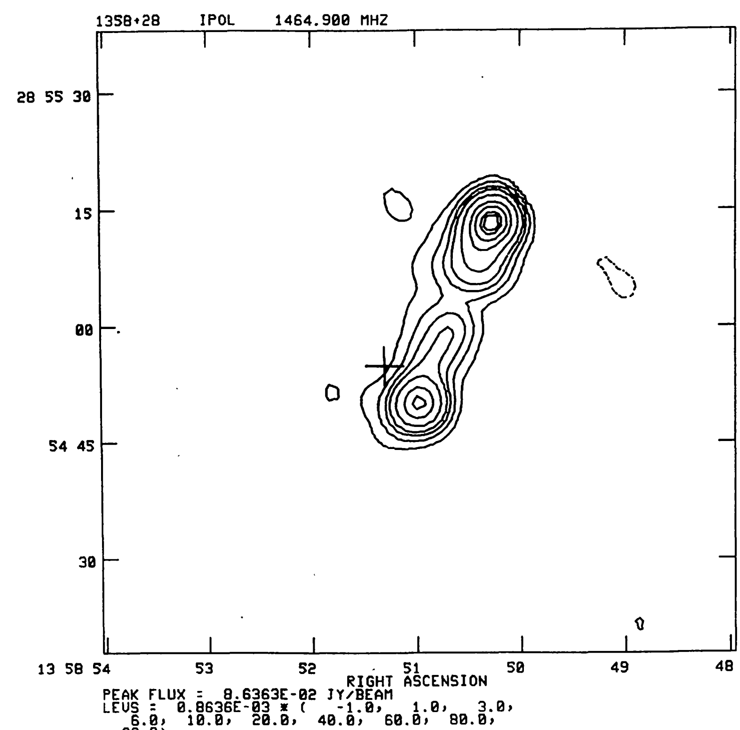

FIGURE 1b (10)

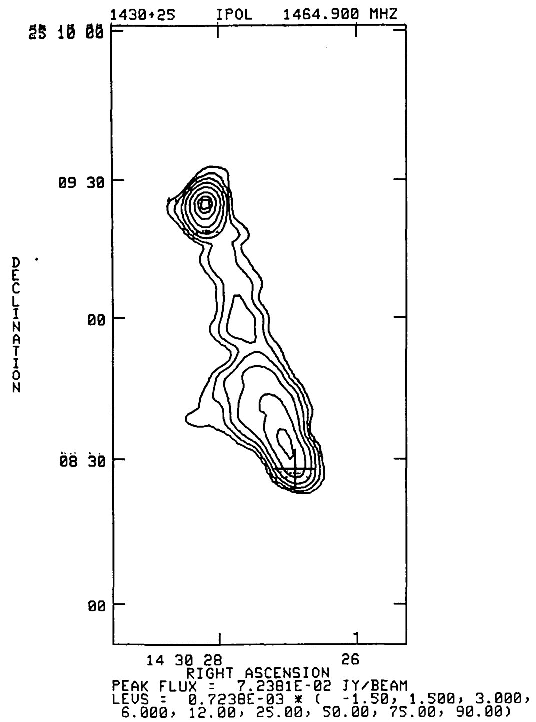

FIGURE 1b (11)

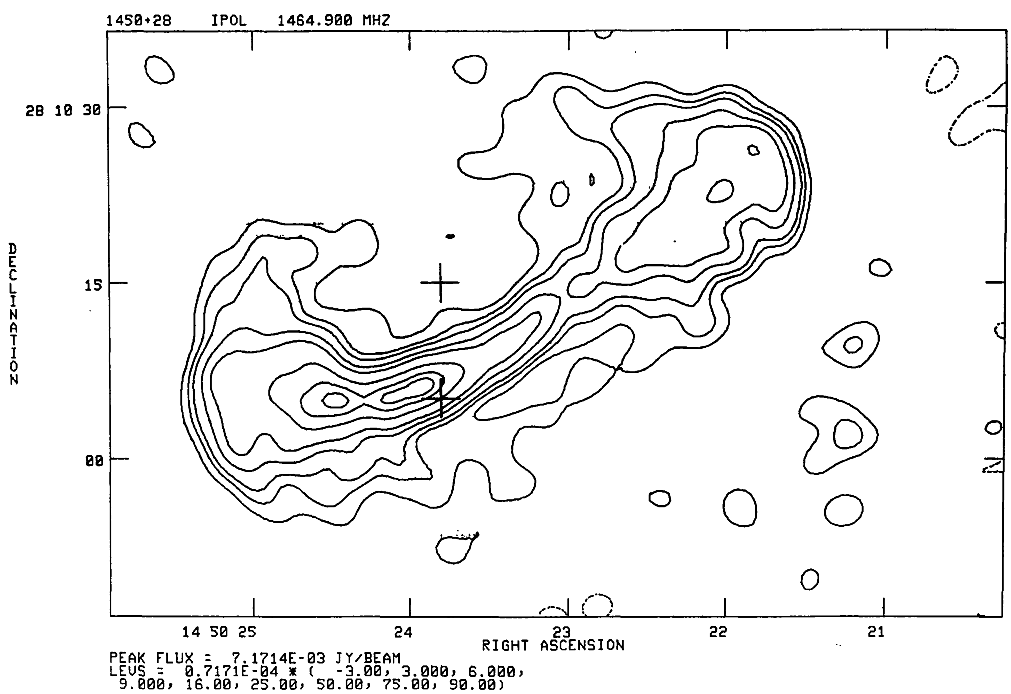

FIGURE 1b (12)

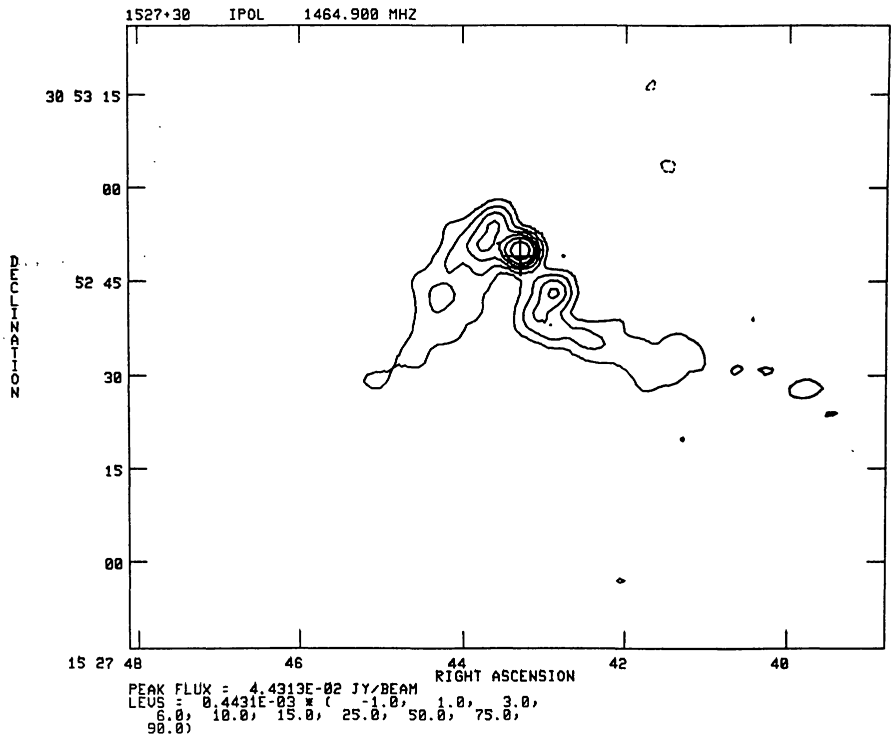

FIGURE 1b (13)

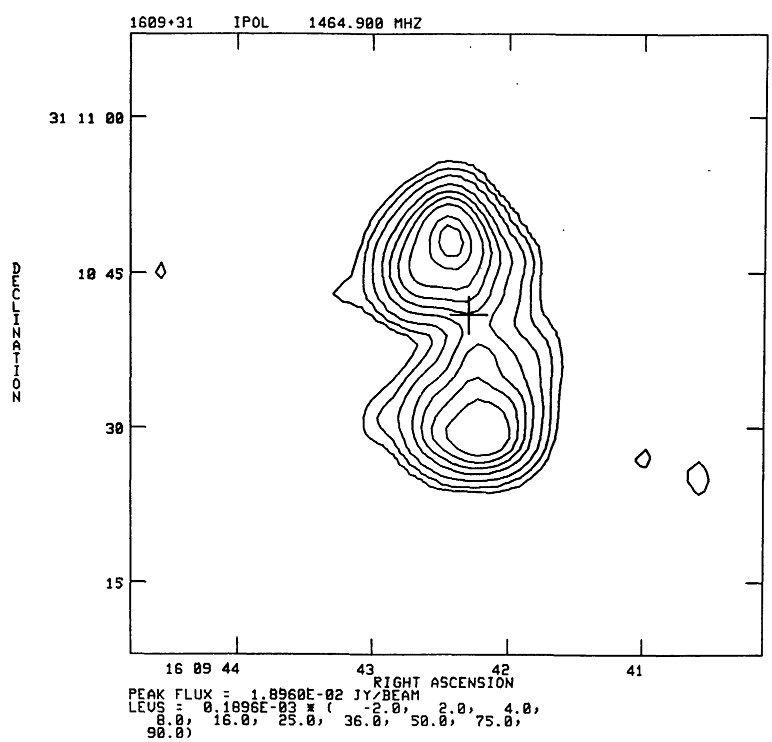

FIGURE 1b (14)

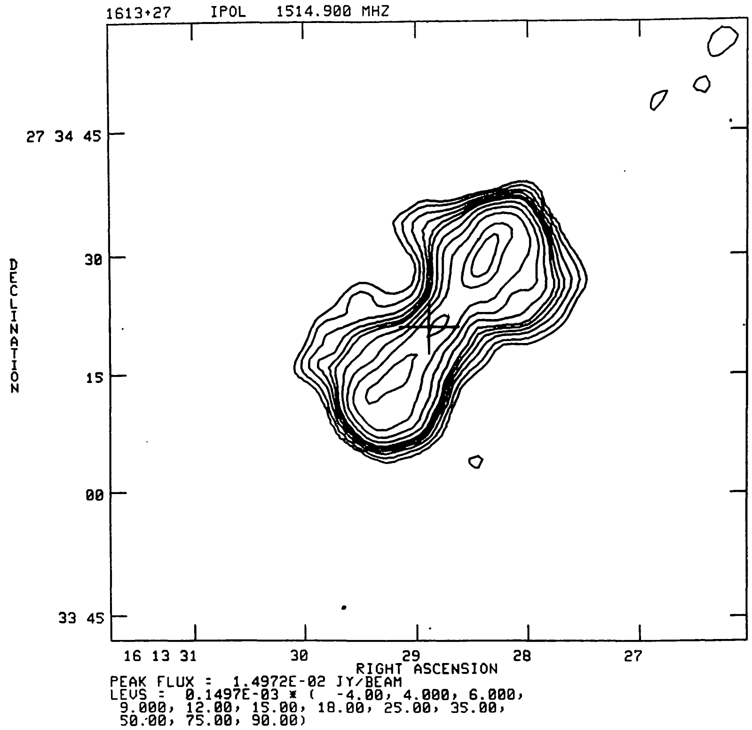

FIGURE 1b (15)

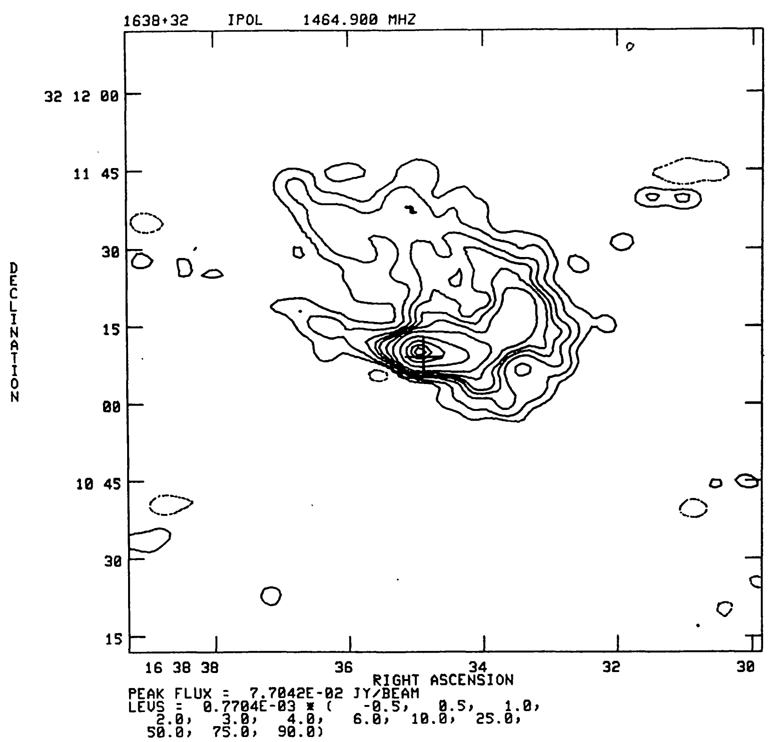

FIGURE 1b (16)

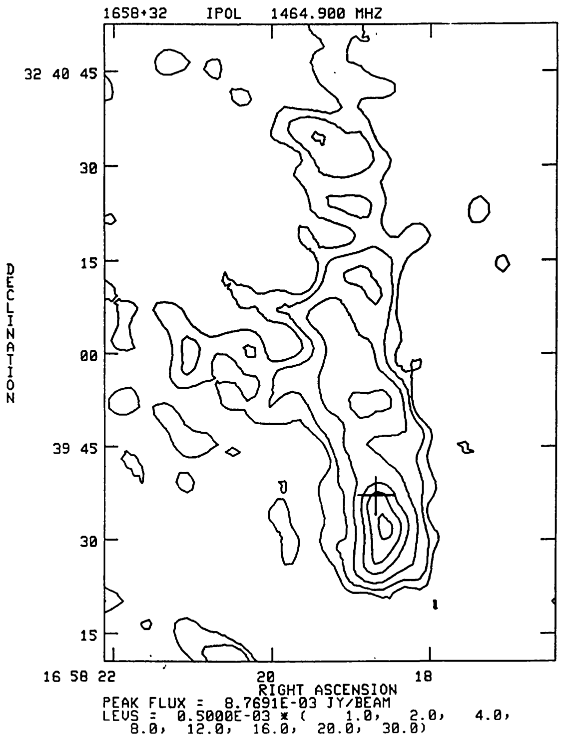

FIGURE 1b (17)

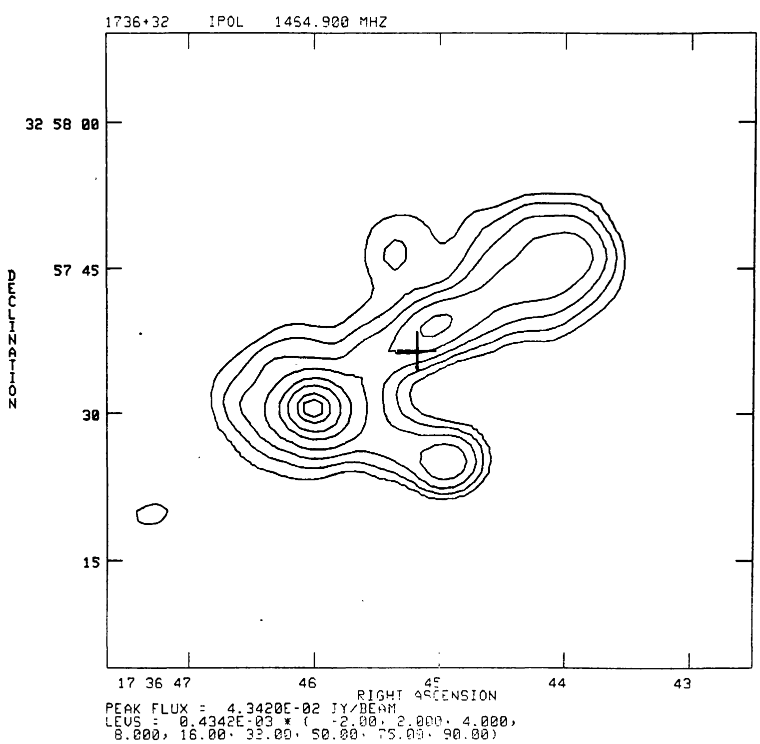

FIGURE 1b (18)

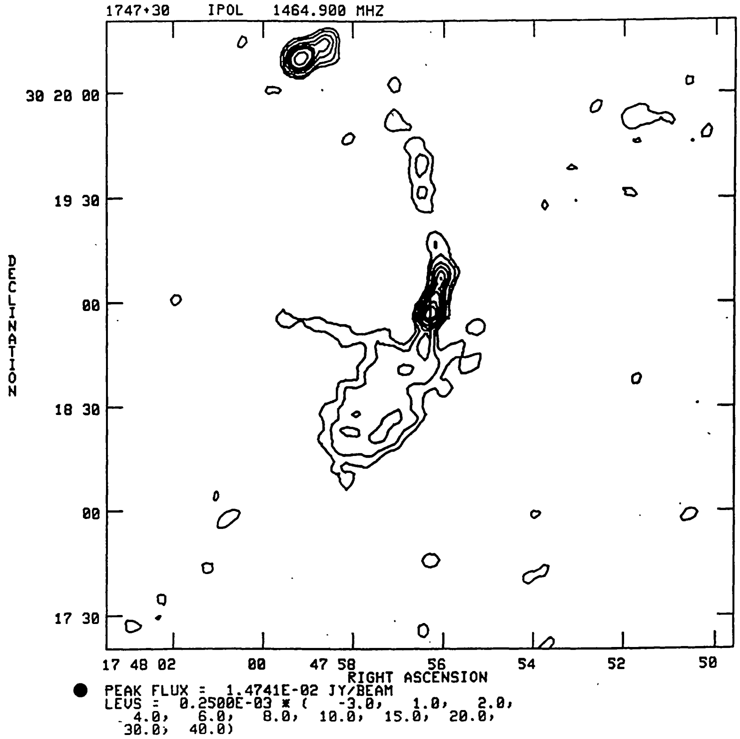

FIGURE 1b (19)

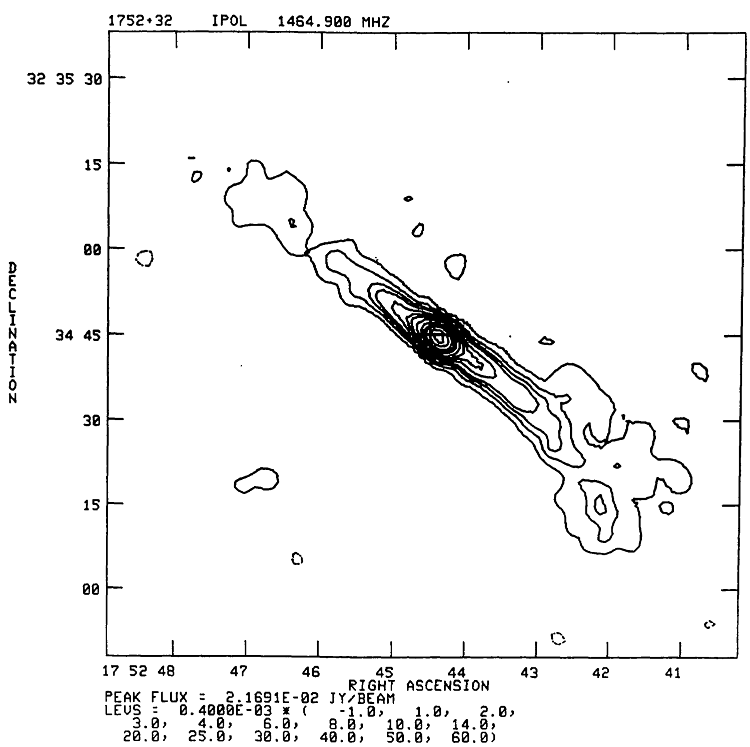

FIGURE 1b (20)